Neurobiology of Disease

Neutral Sphingomyelinase-2 Deficiency Ameliorates Alzheimer's Disease Pathology and Improves Cognition in the 5XFAD Mouse

Michael B. Dinkins,[1] **John Enasko,**[1] **Caterina Hernandez,**[2] **Guanghu Wang,**[1] **Jina Kong,**[1] **Inas Helwa,**[3] **Yutao Liu,**[3] **Alvin V. Terry Jr.,**[2] **and Erhard Bieberich**[1]

[1]Department of Neuroscience and Regenerative Medicine, [2]Department of Pharmacology and Toxicology, and [3]Department of Cellular Biology and Anatomy, The Medical College of Georgia, Augusta University, Augusta, Georgia 30912

Recent evidence implicates exosomes in the aggregation of Aβ and spreading of tau in Alzheimer's disease. In neural cells, exosome formation can be blocked by inhibition or silencing of neutral sphingomyelinase-2 (nSMase2). We generated genetically nSMase2-deficient 5XFAD mice (*fro;*5XFAD) to assess AD-related pathology in a mouse model with consistently reduced ceramide generation. We conducted *in vitro* assays to assess Aβ_{42} aggregation and glial clearance with and without exosomes isolated by ultracentrifugation and determined exosome-induced amyloid aggregation by particle counting. We analyzed brain exosome content, amyloid plaque formation, neuronal degeneration, sphingolipid, Aβ_{42} and phospho-tau levels, and memory-related behaviors in 5XFAD versus *fro;*5XFAD mice using contextual and cued fear conditioning. Astrocyte-derived exosomes accelerated aggregation of Aβ_{42} and blocked glial clearance of Aβ_{42} *in vitro*. Aβ_{42} aggregates were colocalized with extracellular ceramide *in vitro* using a bifunctional ceramide analog preloaded into exosomes and *in vivo* using anticeramide IgG, implicating ceramide-enriched exosomes in plaque formation. Compared with 5XFAD mice, the *fro;*5XFAD mice had reduced brain exosomes, ceramide levels, serum anticeramide IgG, glial activation, total Aβ_{42} and plaque burden, tau phosphorylation, and improved cognition in a fear-conditioned learning task. Ceramide-enriched exosomes appear to exacerbate AD-related brain pathology by promoting the aggregation of Aβ. Reduction of exosome secretion by nSMase2 loss of function improves pathology and cognition in the 5XFAD mouse model.

Key words: 5XFAD; Alzheimer's; ceramide; exosomes; fear conditioning; sphingomyelinase

---

Significance Statement

We present for the first time evidence, using Alzheimer's disease (AD) model mice deficient in neural exosome secretion due to lack of neutral sphingomyelinase-2 function, that ceramide-enriched exosomes exacerbate AD-related pathologies and cognitive deficits. Our results provide rationale to pursue a means of inhibiting exosome secretion as a potential therapy for individuals at risk for developing AD.

Introduction

Alzheimer's disease (AD) is characterized by the accumulation of neurotoxic and gliotoxic amyloid-β (Aβ) peptides processed

from the amyloid precursor protein (APP) by a series of proteases. Another hallmark of AD is the accumulation of highly phosphorylated forms of the microtubule-associated protein tau (p-tau), a chief component of neurofibrillary tangles (Bertram and Tanzi, 2008). Although alternative hypotheses are being examined, it is still widely accepted that Aβ accumulation is the primary cause for the development of AD (Musiek and Holtzman, 2015). However, strategies used to date to prevent Aβ formation or secretion have not been successful. The inability to

interrupt amyloid plaque nucleation and propagation to enhance Aβ clearance represents a critical barrier to progress in AD prevention or treatment.

Ceramides are membrane lipids comprised of a long-chain base (sphingosine) with an amide linkage to a fatty acid. Ceramides can be synthesized *de novo* in the endoplasmic reticulum or generated from the hydrolysis of sphingomyelin by sphingomyelinases in the cytosol or endolysosomal compartments. Ceramide is known to play a number of roles, including cellular stress response (Nikolova-Karakashian and Rozenova, 2010), apoptosis (Shamseddine et al., 2015), and inflammation (Gomez-Muñoz et al., 2016), and can be upregulated in cells by proinflammatory cytokines elevated in AD (Dbaibo et al., 1993; Mathias et al., 1993; Rubio-Perez and Morillas-Ruiz, 2012). Ceramide is elevated in human brain during AD and is proposed to be a predictive serum biomarker (Alessenko et al., 2004; Satoi et al., 2005; Marks et al., 2008; Wang et al., 2008; Mielke et al., 2010; Filippov et al., 2012; Mielke et al., 2012).

As a consequence of elevated ceramide, neural cells release exosomes, nanoscale (40–150 nm diameter) vesicles that are generated by inward budding of the limiting membrane of multivesicular endosomes (MVEs) and released from cells when MVEs fuse with the plasma membrane (Trajkovic et al., 2008; Kowal et al., 2014). The study of exosomes has emerged as a new field in bioscience that may have particular importance for AD. Evidence collected to date suggests that an elevation of exosomes in the brain may play an active role in AD progression (Asai et al., 2015; Joshi et al., 2015) and that a concomitant elevation of Aβ-positive exosomes in the serum could serve as an early biomarker of AD (Fiandaca et al., 2015). Aβ and APP C-terminal fragments have been shown to be secreted in association with exosomes from various sources (Rajendran et al., 2006; Sharples et al., 2008; Perez-Gonzalez et al., 2012) and exosomes can accelerate Aβ aggregation (Yuyama et al., 2012; Dinkins et al., 2014; Falker et al., 2016). Exosome secretion can be significantly reduced in neural cell types by inhibiting or silencing neutral sphingomyelinase-2 (nSMase2) (Trajkovic et al., 2008; Yuyama et al., 2012; Dinkins et al., 2014; Asai et al., 2015), which can also suppress glial activation (Kobayashi et al., 2012; Wang et al., 2012; Gu et al., 2013). It is not known whether genetic ablation of nSMase2 has beneficial effects on AD progression and cognition in aging mice. Here, we show for the first time that reducing exosomes through nSMase2 deficiency by crossing in the *fragilitas ossium* (*fro/fro;* denoted simply as *fro* in this work) allele (Guénet et al., 1981) to the 5XFAD mouse model, which normally exhibits accelerated Aβ plaque formation, alleviates the progression of Aβ pathology and improves cognition.

Materials and Methods

Animals and reagents. To generate *fro;*5XFAD mice, we crossed 5XFAD mice (Oakley et al., 2006; SJL background; The Jackson Laboratory) with the *fro* mouse (C3H background; gift from Dr. Christophe Poirier, Indiana University, Indianapolis), which carries a deletion in the sphingomyelin phosphodiesterase-3 gene that encodes nSMase2 (NCBI gene ID: 58994; Aubin et al., 2005). Mice were handled according to the National Institutes of Health's *Guide for the Care and Use of Laboratory Animals*. All procedures involving mice were approved by the Augusta University Institutional Animal Care and Use Committee.

Aβ42 and HiLyte488-Aβ42 were purchased from AnaSpec, dissolved in 1% ammonia, and diluted in PBS to 1 mg/ml. Rabbit anticeramide IgG for immunohistochemistry was generated in our laboratory (Krishnamurthy et al., 2007). PHF-1 antibody (anti-pS396/404-tau) was a gift from Dr. Peter Davies (Albert Einstein College of Medicine, New York, NY), and anti-pS262-tau (44–750G) was from Biosource. Anti-Aβ antibodies were from ThermoFisher (rabbit monoclonal, H31L21) and Mil-

lipore (mouse, 4G8). Antibodies against TSG101 (C-2), Alix (1A12), glial fibrillary acidic protein (GFAP; C-19), actin (C-2), and total Tau (Tau46) were from Santa Cruz Biotechnology. Horseradish peroxidase (HRP)-conjugated cholera toxin B subunit was from Sigma-Aldrich. All secondary antibodies were from Jackson ImmunoResearch. Anti-CD11b and anti-ACSA2 magnetic microbeads and columns were obtained from Miltenyi Biotec. Ceramides, including pacFA-ceramide [N-(9-(3-pent-4-ynyl-3-H-diazirin-3-yl)-nonanoyl)-D-*erythro*-sphingosine], were from Avanti Polar Lipids. FluoroJade B was from Histo-Chem and ExoQuick was from System Biosciences.

Primary cell culture. Glial cultures were prepared from pooled male and female C57BL/6 (The Jackson Laboratory) P0 mouse cortices and cultured in DMEM + 10% fetal bovine serum (Atlanta Biologicals) as described previously (Wang et al., 2008). For Aβ clearance assays, glial cultures were labeled with Anti-ACSA2 or anti-CD11b microbeads to separate astrocytes and microglia, respectively, through a magnetic column (Miltenyi) before culture in 12-well plates. For exosome collection, astrocytes were passed to 100 mm plates and, when confluent, changed to serum-free DMEM containing 50 μM of the sphingomyelin synthase inhibitor D609 to raise ceramide levels and stimulate exosome secretion.

Exosome preparation and analysis. Exosomes were harvested from conditioned medium by differential ultracentrifugation as described previously (Guescini et al., 2010; Wang et al., 2012) and resuspended in serum-free DMEM for Aβ clearance assays. For Western blot analysis, exosomes were resuspended directly in 2× SDS sample buffer (Sigma-Aldrich). Serum exosomes were isolated using ExoQuick as directed by the manufacturer's protocol (Taylor et al., 2011) and resuspended in 2× SDS sample buffer. For nanoparticle tracking analysis (NTA) with the ZetaView PMX110 (Particle Metrix) system (Mehdiani et al., 2015), exosomes were resuspended and diluted in PBS. Polystyrene beads (100 nm) were used for instrumental calibration. Two-milliliter diluted samples were injected into the ZetaView cell and NTA measurements were recorded at 11 positions with two cycles each position. Acquisition parameters were as follows: temperature 23°C, sensitivity 70, 30 frames/s, shutter speed 100, and laser pulse duration equal to that of shutter duration.

Brain dissociation for extracellular vesicle analyses. Adult male 5XFAD and *fro;*5XFAD mice were perfused with PBS after anesthesia to eliminate serum vesicles and whole brains were dissected. Tissue dissociation was performed using the gentleMACS Octodissociator and the Adult Brain Dissociation Kit (Miltenyi Biotec) according to the manufacturer's protocol to reduce variability of tissue homogenates. Briefly, brain tissue was minced and digested with a proprietary enzyme solution on the gentleMACS dissociator adult brain program. The dissociated tissue was diluted with PBS containing calcium and magnesium and subjected to differential ultracentrifugation as described previously (Perez-Gonzalez et al., 2012). Briefly, cellular suspensions were successively centrifuged at $300 \times g$ (10 min), $2000 \times g$ (10 min), and $20,000 \times g$ (30 min) and then passed through a 0.2 μm filter before ultracentrifugation at $110,000 \times g$ (90 min). The resulting pellets were resuspended in PBS for downstream analyses.

Lipid analyses. For ceramide analysis, lipids were extracted from vesicles, cells, and tissue using the Folch extraction method with 2:1 chloroform:methanol (Folch et al., 1957). Brain tissue ceramides of different fatty-acyl chain lengths and other sphingolipids were quantified using LC-MS/MS by the lipidomics core facility at the Medical University of South Carolina, Charlston (Dr. Jacek Bielawski, director). For thin-layer chromatography (TLC) and dot blots, extracted lipids from vesicles and cells were dried under nitrogen and subsequently resolubilized (chloroform:methanol, 1:1 for TLC; ethanol:PBS, 1:1 for dot blots). TLC plates were loaded as to normalize lipid to protein or cholesterol as indicated, developed using chloroform:methanol:glacial acetic acid (95:4.5:0.5), and visualized by charring with 3% cupric acetate (w/v) in 8% phosphoric acid (v/v). Dot blots were probed with HRP-cholera toxin B subunit to bind GM1.

Sample preparation for ELISA, histochemistry, and immunolabeling analyses. Brains from both male and female mice were divided in half down the midline for ELISA and sectioning. The human Aβ42 ELISA kit (ThermoFisher) was used according to the manufacturer's protocol to

measure $A\beta_{42}$ in brain tissue. $A\beta$ plaques were labeled in frozen, fixed brain tissue with thioflavin-S as described in detail previously (Dinkins et al., 2014; Dinkins et al., 2015). FluoroJade B staining and immunolabeling of fixed cells and brain tissue were also performed as described previously (Wang et al., 2008; Wang et al., 2012; Dinkins et al., 2014). For cells incubated with pacFA-ceramide, all procedures before UV cross-linking were performed in the dark. pacFA-ceramide was loaded into astrocytes at 5 μM (diluted 1:1000 from a stock in 98% ethanol + 2% dodecane) for 5 h and then washed. After 24 h of additional culture, astrocytes were treated with 0.5 μM Hi-Lyte488 $A\beta_{42}$ with or without pacFA-ceramide-loaded exosomes. The cells receiving pacFA-ceramide-preloaded exosomes were not previously exposed to pacFA-ceramide. After 12 h, the cultures received fresh medium and were cross-linked by UV irradiation (365 nm for 5 min) at room temperature. Control cells did not receive UV irradiation. All cells were fixed with ice-cold methanol and washed with 1:1 chloroform:methanol and finally with methanol, which removes non-cross-linked pacFAceramide and other lipids. Cross-linked pacFA-ceramide was fluorescently labeled with Alexa Fluor 647 azide using a click reaction as described previously (Kong et al., 2015) before other immunolabeling.

$A\beta$ clearance assays. Astrocytes or microglia were cultured in 12-well plates to confluency. Astrocyte exosomes were resuspended in serum-free DMEM and preincubated with 2.5 μM $A\beta_{42}$ at 37°C (200 μl). After 5 h, $A\beta$ with and without exosomes was added to glial cultures in serum-free DMEM for 4 or 18 h (1 ml total, 0.5 μM final $A\beta$ concentration). Cells were washed 3× with warm PBS and prepared for ELISA by lysis in a 1% Triton X-100 lysis buffer containing protease inhibitor mixture (Sigma-Aldrich). To remove surface-associated $A\beta$, cells were treated with 0.05% trypsin treatment for 3 min and then washed 3× with PBS before ELISA (Verghese et al., 2013). Protein content was measured by the Lowry method (RC-DC assay kit; Bio-Rad).

Contextual and cued fear conditioning and shock threshold. Fear-conditioned associative learning was assessed in male mice and analyzed (double-blinded) as described previously (Dineley et al., 2002). Briefly, mice were introduced into a novel environment (sound-attenuated chamber; Med Associates). After a 3 min exploration period, a 30 s white noise acoustic (cued) stimulus was presented, followed by the delivery of a scrambled 2 s electric shock (0.5 mA, contextual stimulus) to the floor grid. A second acoustic and electric shock stimulus pairing was initiated after 2 min and the session ended after an additional 2 min exploration period. After 24 h, the mice were returned to the same environment for 5 min to assess contextual fear learning. After a 4 h rest period, the mice were placed in a novel environment for a 3 min exploration period, followed by the presentation of same acoustic (white noise) stimulus on the day prior for an additional 3 min to assess cued fear learning. All sessions were video recorded and freezing behavior was assessed and scored every 5 s to report the percentage of freezing per session in total or 1 min bins. To validate fear-conditioning data, sensory perception of all fear conditioning-tested mice was determined by shock threshold examination. Mice received single shocks in the environment used for training and contextual fear testing. Shocks were delivered every 30 s beginning at 0.1 mV up to 0.7 mV and mice were monitored for vocalization, flinching, and scattering behaviors. No further shocks were delivered once an animal displayed jumping or scattering behavior.

Statistical analyses. To analyze amyloid plaques, images were taken of the retrosplenial, somatosensory, motor, and auditory cortex (four sections per animal) and analyzed with ImageJ (blinded) for plaque number, plaque area, and average plaque size. Western blot and TLC bands were also quantified using ImageJ. Data were analyzed using GraphPad Prism by t test, one-way, or two-way ANOVA as appropriate with Bonferroni *post hoc* testing. All p-values are shown in the figures.
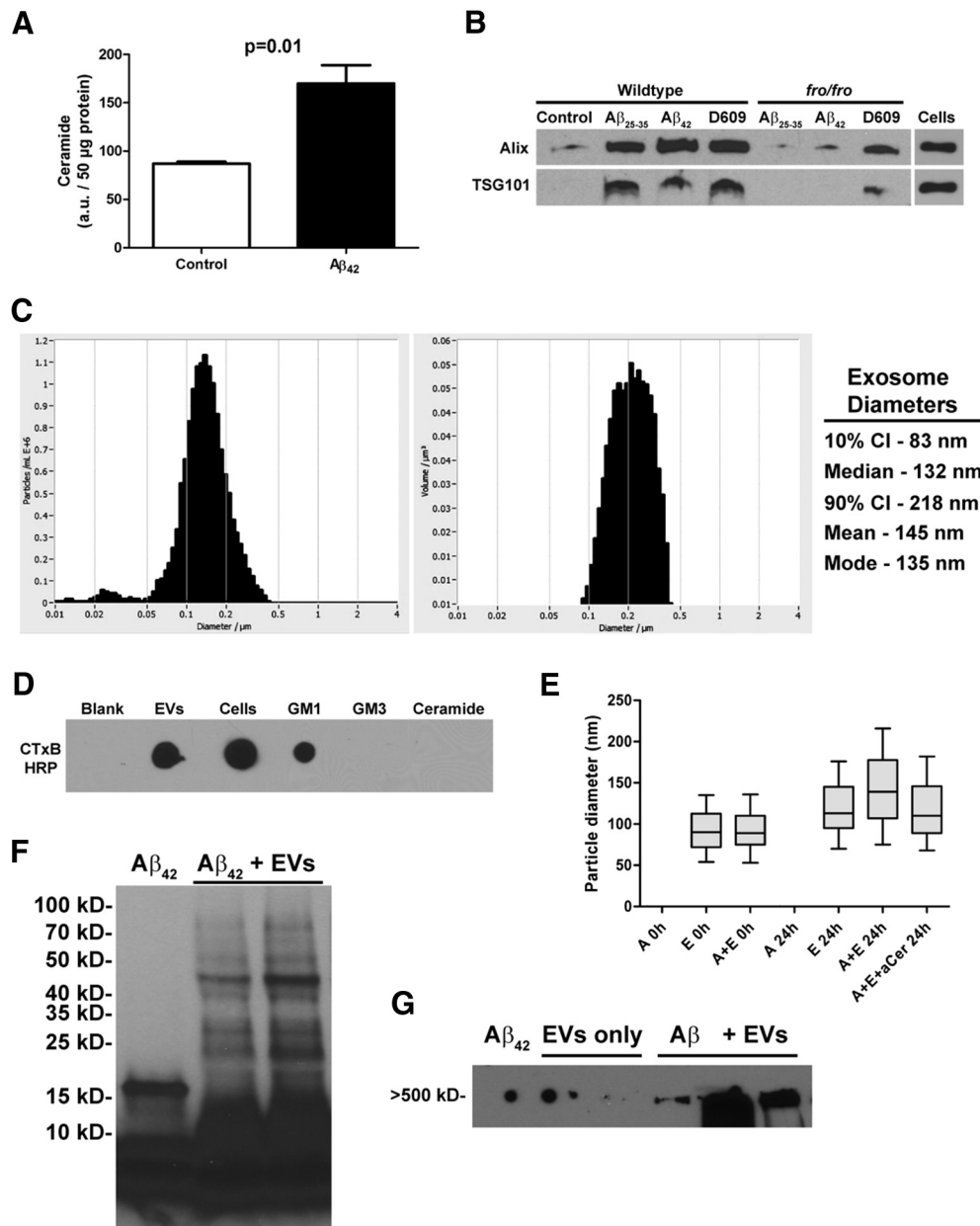
Results

Brain-cell-derived exosomes promote $A\beta$ aggregation and reduce glial $A\beta$ clearance

Increases in astroglial ceramide are known to affect neuron function negatively in AD and mouse models (Satoi et al., 2005; Patil et al., 2007; Jana and Pahan, 2010). We previously reported ele-

vated astrocyte ceramide levels in an AD mouse model (Wang et al., 2008) and, when challenged with $A\beta_{25-35}$ *in vitro*, astrocytes secrete ceramide-enriched exosomes (Wang et al., 2012). We show here that *in vitro*-cultured primary mouse astrocytes treated with 1 μM $A\beta_{42}$ doubled their ceramide levels (Fig. 1A) and up-regulated secretion of exosomes as quantified using Western blot analysis of ESCRT and related proteins associated with endosomal transport and present in secreted vesicles (Alix, TSG101; Fig. 1B) and ZetaView NTA (data not shown). nSMase2-deficient *fro* astrocytes did not respond with exosome secretion to $A\beta$ challenge. However, both wild-type (WT) and *fro* astrocytes secreted exosomes when treated with the sphingomyelin synthase inhibitor D609 (Fig. 1B), which elevates ceramide levels synthesized *de novo* (Luberto and Hannun, 1998; Dinkins et al., 2014). ZetaView NTA revealed that the majority of vesicles secreted by astrocytes to be between 83 and 218 nm in diameter with a median/mode of 132/135 nm, consistent with a population of exosomes (Fig. 1C). In addition, we found that GM1, a ganglioside shown to be important in neuronal exosome-stimulated $A\beta$ aggregation (Yuyama et al., 2012; Yuyama et al., 2015), $A\beta$-seeding (Hayashi et al., 2004), and sequestration of $A\beta$ oligomers (Hong et al., 2014) was enriched in astrocyte exosomes as determined by dot-blot analysis of exosome pellets and whole astrocytes using the cholera toxin B subunit as a probe (Fig. 1D). Astrocyte exosomes also stimulated the aggregation of $A\beta$. Using ZetaView NTA, we determined that the diameter of exosomes incubated for 24 h with $A\beta_{42}$ was increased by ~30% compared with exosomes held in buffer, which corresponds to a particle volume increase of 2.2-fold (Fig. 1E). This increase in exosome diameter was blocked by an anticeramide antibody (Fig. 1E), which can be used to isolate exosomes and other ceramide-enriched vesicles (He et al., 2012; Wang et al., 2012). Western blot analysis also showed that astroglial exosomes promoted the appearance of $A\beta$ in various oligomeric forms (Fig. 1F, lanes 2 and 3), which was previously unreported, as well as higher-molecular-weight species (Fig. 1G). The published literature contains examples of interchangeable use of the terms "exosome" (smaller, secreted vesicles) and "microvesicles" (shed vesicles, which tend to be larger in size and pellet at 10,000 to 20,000 × g), with others using the more generic term "extracellular vesicles" (EVs). Our NTA and molecular analyses indicate isolation of a mostly exosomal population based on centrifugation conditions that remove larger microvesicles before ultracentrifugation or ExoQuick-based isolation and also on markers of four EV populations reported in a recent proteomic study (Kowal et al., 2016). We will refer to our preparations as both exosomes and EVs because there is currently no method available to ensure the isolation of a specific population of vesicles.

We then investigated whether ceramide-enriched EVs associated with $A\beta$ aggregates *in vitro* and *in vivo*. Using an anticeramide IgG (Krishnamurthy et al., 2007), we regularly found $A\beta_{42}$-containing plaques in the 5XFAD mouse brain surrounded by GFAP-positive reactive astrocytes that had a dense ceramide core (Fig. 2A). Because it was shown previously that exosomal proteins accumulated in the plaques of AD patients (Rajendran et al., 2006), it is likely that this dense ceramide labeling (Fig. 2A) is due to the presence of ceramide-enriched exosomes acting as a seed for plaque formation. We investigated this phenomenon with astrocytes *in vitro* using a bifunctional ceramide analog, pacFA-ceramide (pacFA-cer), which has been used previously in our laboratory (Kong et al., 2015). The fatty acid of pacFA-cer contains a terminal alkyne group for Click chemistry labeling and a diazirine group for UV cross-linking to ceramide-binding pro-

A

B

C

Exosome Diameters

10% CI - 83 nm
Median - 132 nm
90% CI - 218 nm
Mean - 145 nm
Mode - 135 nm

D

E

F

G

Figure 1. Astrocyte-derived exosomes accelerate aggregation of $A\beta_{42}$. **A**, Quantification of ceramide by densitometry of high-performance thin-layer chromatography after 24 h exposure of primary astrocytes to 1 μM $A\beta_{42}$ ($n = 3$). **B**, Western blot analysis of exosome markers Alix and TSG101 from WT and *fro/fro* astrocytes after differential ultracentrifugation of conditioned medium. Lanes represent pellets from equivalent amount of medium. **C**, Representative histograms showing ZetaView-measured (left) particle concentration (y-axis) versus diameter (x-axis) and (right) volume (y-axis) versus diameter of astrocyte exosomes with descriptive statistics listed on the right. **D**, Dot-blot comparison of astrocyte- and exosome-derived lipids and standards probed with cholera toxin B subunit to detect GM1 ganglioside. **E**, ZetaView-measured particle diameter of exosomes alone or in the presence of $A\beta_{42}$ with and without anticeramide IgG. Box plots show median diameter, with bars indicating the 10th to 90th percentile range ($n = 3$). **F, G**, Western blot analyses of $A\beta_{42}$ after incubation alone or in the presence of exosomes showing various aggregation states. Lines above the blot images indicate multiple samples run side by side (in **F**, $n = 2$ samples of $A\beta$+ EVs; in **G**, 2 lanes of EVs only and 3 lanes of $A\beta$+ EVs). In **G**, the spots on the left side of the blot image are due to nonspecific background.

teins. Cells loaded with pacFA-cer, but that were not UV cross-linked, showed no Click reaction-dependent labeling (Fig. 2B), whereas cells exposed to UV light showed labeling of plasma membrane and intracellular structures (Fig. 2C and unpublished observations). A third group of astrocytes were not exposed to pacFA-cer directly, but were exposed to pacFA-cer-loaded EVs (loaded separately under the same conditions as cells). At the same time pacFA-cer-loaded EVs were added to cells, 0.5 μM Hi-Lyte488-$A\beta_{42}$ ($A\beta$-488) was added to all three groups. In the absence of EVs, we observed $A\beta$-488 aggregates (5–20 μm diameter) associated with the plasma membrane of astrocytes (Fig.

2B,C; see orthogonal views in Fig. 2G showing the bulk of $A\beta$ is not in plane with intracellular components), as well as colocalizing with lysosomes (LysoTracker Red DND-99; Fig. 2E). In the presence of pacFA-cer-loaded EVs, we observed dense aggregates of $A\beta$-488 that colocalized with pacFA-cer, indicating that the pacFA was cross-linked to proteins in the EVs (Fig. 2D,G). We did not observe any differences in colocalization of $A\beta$-488 with LysoTracker in the presence of EVs, although there appeared to be comparatively more extracellular $A\beta$-488 aggregates in these samples (Fig. 2F). Quantification of $A\beta$-488 signal from 20× confocal projections of these cultures showed an ~5-fold in-
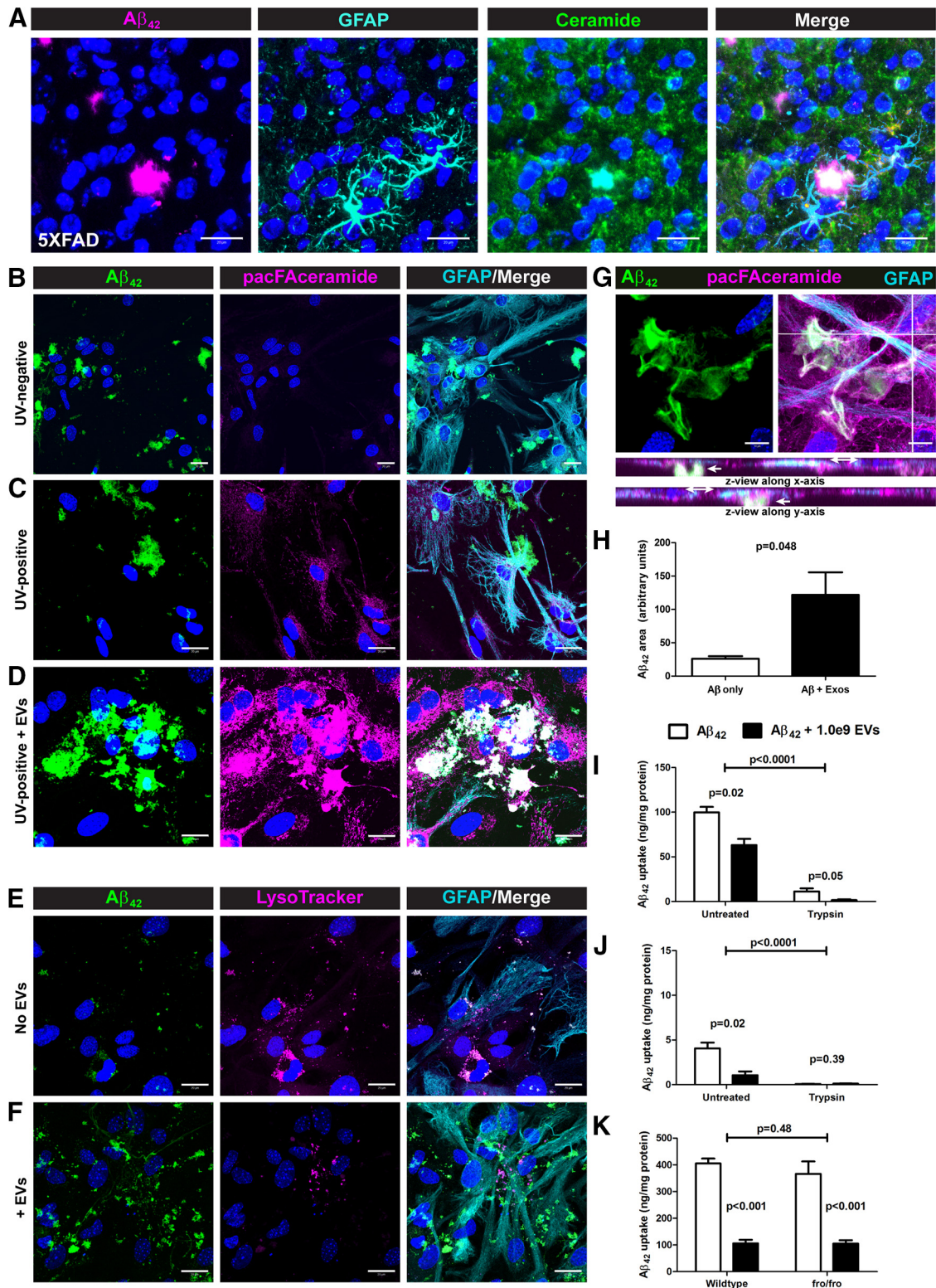
Figure 2. Ceramide-enriched exosomes accelerate Aβ deposition at the cell surface and reduce glial Aβ clearance *in vitro*. ***A***, Confocal micrographs of brain tissue from 10-month-old 5XFAD mice labeled for Aβ$_{42}$, ceramide and GFAP as indicated showing ceramide localization at the core of Aβ$_{42}$ plaques. ***B–D***, Confocal projections of cultured astrocytes exposed to HiLyte488-Aβ$_{42}$ after preloading with pacFA-ceramide (***B***, ***C***) or upon concomitant addition of pacFA-ceramide-loaded EVs (***D***); pacFA-ceramide was labeled by Click reaction with Alexa Fluor 647-azide followed by GFAP immunolabeling. ***E***, ***F***, Confocal projections of cultured astrocytes exposed to HiLyte488-Aβ$_{42}$ in the absence (***E***) or presence (***F***) of EVs and labeled with LysoTracker Red DND-99 followed by GFAP immunolabeling. ***G***, Confocal micrograph of cultured astrocytes labeled pacFA-ceramide (Alexa Fluor 647) and immunolabeled for GFAP and Aβ$_{42}$ with orthogonal views to indicate extracellular and intracellular planes. Scale bars: ***A–F***, 20 μm; ***G***, 10 μm. ***H***, Quantification of Aβ$_{42}$ aggregate size (area) from 20× views (data not shown) of confocal micrographs of astrocytes exposed to HiLyte488-Aβ$_{42}$ in the absence and presence of EVs ($n = 3$, Student's *t* test). ***I–K***, Aβ$_{42}$ ELISA data (uptake) after Aβ *in vitro* clearance assays with mixed glial cultures (***I***, ***K***) and astrocytes (***K***) ($n = 3$ each, 2-way ANOVA with Bonferroni *post hoc* test). All quantitative data shown are means ± SEM.

crease in extracellular aggregated Aβ in the presence of EVs (Fig. 2H). We next determined the ability of cultivated glia to clear Aβ_{42} after incubation with astrocyte-derived exosomes. Consistent with the above results, mild trypsin treatment of glial cells before harvest (Verghese et al., 2013) demonstrated that the majority of Aβ_{42} was present in the extracellular space (Fig. 2I–K). ELISA of mixed glial (astrocytes and microglia) lysates analyzed after 4 h of incubation with Aβ_{42} with and without EVs showed that cells incubated in the absence EVs were associated with more Aβ than cells that received EVs. Trypsin treatment significantly reduced the amount of Aβ_{42} detected by ELISA, indicating that most of the Aβ was present extracellularly (Fig. 2I). After a 4 h incubation, the majority of Aβ in culture would not have been degraded by either lysosomes or secreted proteases. After 18 h, there was still more Aβ associated with the cells cultured in the absence of EVs that did not receive trypsin treatment, whereas intracellular Aβ was only detectable slightly above background level for trypsin-treated cells (see Fig. 2J for astrocytes; microglia not shown). We confirmed these results using mixed glial cells from *fro* mice, which do not respond to Aβ by elevating intracellular ceramide or undergoing apoptosis (Fig. 1B; Wang et al., 2012). WT and *fro* cells showed no difference in Aβ_{42} clearance in the absence of EVs, whereas cells of both genotypes showed reduced Aβ clearance in the presence of EVs, but were not different from each other (Fig. 2K). Because *fro* cells did not clear Aβ_{42} differently from WT cells in the presence or absence of EVs, we pursued our further studies in *fro* mice to address the question of whether exosomes contribute to AD pathology *in vivo*.

*fro;*5XFAD mice have reduced brain EVs, ceramides, and serum anticeramide IgG levels

To address the question of whether nSMase2-dependent EVs are involved in the development of AD pathology *in vivo*, we crossed the 5XFAD mice with *fro/fro* mice, which are deficient in nSMase2, the predominant nSMase expressed in mouse brain (Liu et al., 1998; Tomiuk et al., 2000), to generate homozygous *fro* mice bearing the 5XFAD transgenes (*fro;*5XFAD). These *fro* mice completely lack functional nSMase2 (Aubin et al., 2005) and are hypothesized to be deficient in ceramide-enriched exosomes, with this enzyme playing a key role in exosome formation and secretion (Trajkovic et al., 2008; Yuyama et al., 2012; Kosaka et al., 2013; Dinkins et al., 2014). We isolated brain exosomes after PBS perfusion of 5XFAD and *fro;*5XFAD mice using the gentleMACS Octodissociator based on the method of Perez-Gonzales et al. (Perez-Gonzalez et al., 2012) with modifications. ZetaView NTA particle size distribution profiles show a marked difference in abundance of EVs at various sizes, with those from *fro;*5XFAD mice being fewer in total number but also shifted to right in size distribution (Fig. 3A with modes of 100 nm for 5XFAD and 120 nm for *fro;*5XFAD). When total EVs were quantified by NTA, the *fro;*5XFAD brains showed a reduction to less than half of the total EVs in the 5XFAD brain (Fig. 3B). In addition, the total protein content in the *fro;*5XFAD EV pellets was significantly reduced ($p = 0.01$, data not shown) and there was a reduction in the EV marker flotillin-2 by Western blot in the *fro;*5XFAD mice when normalized to total brain volume (i.e., normalizing to protein content would require loading additional total numbers of vesicles in each lane). We were unable to verify markers such as Alix and TSG101 in the brain EV preparations due to conditions used during their isolation (Fig. 3C, bottom). The gentleMACS adult brain dissociation protocol employs a proprietary mixture, likely containing mild proteases. To confirm this finding, we digested exosomes isolated from astrocyte

cell culture with 1 unit of papain (50°C for 30 min in PBS). Western blots confirmed degradation of TSG101 (Fig. 3D) and Alix (data not shown). To further characterize our isolated brain EVs, we extracted the lipid components for TLC analysis. All samples were spotted on TLC plates and normalized to cholesterol because it has been shown that ceramides are more highly enriched in EVs than cholesterol compared with their parent cells (Record et al., 2014). All brain and astrocyte (for comparison) EV samples were more highly enriched with ceramide per unit cholesterol (Fig. 3E), with whole astrocyte and total brain cell extracts displaying lipids not enriched in their respective EVs. When quantified, the ceramide:cholesterol ratio of *fro;*5XFAD brain was significantly reduced compared with 5XFAD (Fig. 3F, left), but more variable in the EV pellets (Fig. 3F, right). However, *fro;*5XFAD EV ceramide was significantly reduced compared with 5XFAD EVs when normalized to protein (Fig. 3G). Next, we investigated whether nSMase2 deficiency affected the level of serum EVs in 5XFAD and *fro;*5XFAD mice. We have previously used an antibody against the ESCRT-I accessory protein Alix to determine relative quantities of astrocyte and serum exosomes by Western blot because other markers are difficult to quantify due to the presence of high levels of endogenous serum IgG (Dinkins et al., 2014; Dinkins et al., 2015). Although ZetaView NTA gave variable results for serum EVs, we found that *fro;*5XFAD mice had significantly reduced levels of Alix protein in exosome pellets isolated by chemical polymer methods (ExoQuick) or by traditional differential ultracentrifugation (Fig. 3H,I) and normalized by starting serum volume, suggesting reduced Alix-positive EVs in sera of *fro* mice.

It was reported previously that *fro/fro* mouse brain ceramides were reduced by ~60–70% (Qin et al., 2012) and that nSMase2 inhibition lowered total brain ceramides (Tabatadze et al., 2010). We found total ceramide levels in 3-month-old *fro* and *fro;*5XFAD mouse brain to be reduced by ~35–40% compared with WT and 5XFAD mice, respectively (Fig. 4A). The three most abundant ceramides, C18:0, C24:1, and C18:1, are presented in Figure 4, B–D, and in all cases they are significantly reduced in *fro;*5XFAD mice compared with 5XFAD mice. It should be noted that C18:0 and C24:1 ceramide are also the major ceramide species found in exosomes secreted by astrocytes when exposed to Aβ (Wang et al., 2012). Many of the minor ceramide species' levels (e.g., C14:0, C20:1, C24:0) were not significantly different among the genotypes, with the exception of C16:0 (Fig. 4E). Other moderately abundant ceramides (C20:0, C22:1) also showed no differences (Fig. 4F and data not shown, respectively). Interestingly, 5XFAD brains had significantly reduced levels of the neuroprotective lipid sphingosine-1-phosphate (S1P), although total sphingosine levels were not different among the four genotypes (Fig. 4G,H). S1P levels in *fro;*5XFAD mice were similar to WT and *fro* mice (Fig. 4H), suggesting that expression or activity of sphingosine kinases are restored in these animals, although further analyses of this hypothesis is beyond the scope of this study.

We recently reported that 5XFAD mice exhibited an age-dependent increase in serum antibodies that recognized C18:0 and C24:1 ceramides by ELISA (Dinkins et al., 2015). To determine whether reduction of ceramides and/or ceramide-enriched EVs leads to a decrease of the respective antibodies, we measured the relative levels of anticeramide IgG in the sera of 5XFAD, *fro;*5xFAD, and nontransgenic littermates with our rabbit anticeramide IgG for comparison (Krishnamurthy et al., 2007). Using lipid ELISA, we found no differences among groups with respect to serum IgGs recognizing C18:0 sphin-
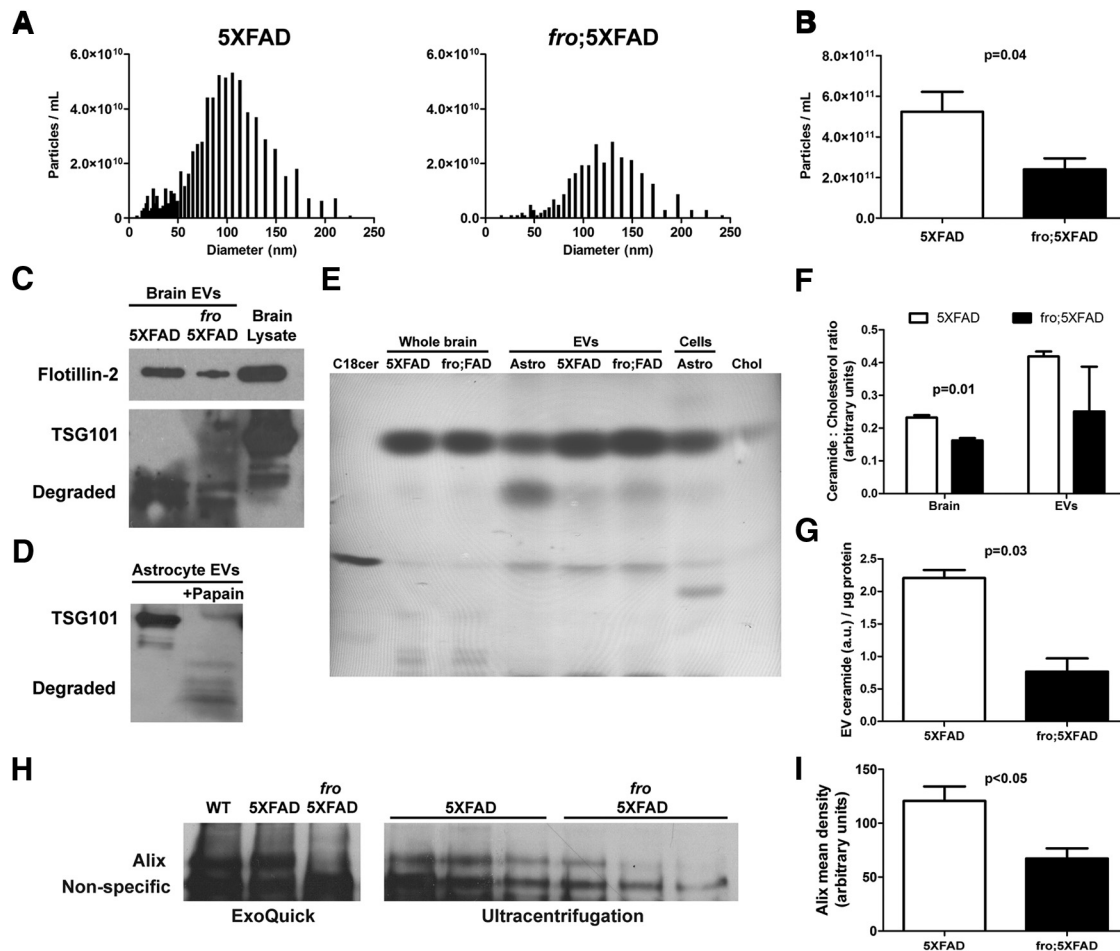
Figure 3. Reduced extracellular vesicles in *fro;*5XFAD mice. *A*, Representative frequency distribution histograms showing ZetaView-measured EV particle concentration (*y*-axis) versus diameter (*x*-axis) from 5XFAD (left) and *fro;*5XFAD (right) mouse brains. *B*, Quantification of EV particles from 5XFAD and *fro;*5XFAD brains (*n* = 4; Student's *t* test). *C, D*, Western blots of EVs isolated from 5XFAD and *fro;*5XFAD brains (*C*) and astrocytes after digestion with papain (*D*). *E*, Representative thin-layer chromatograph of lipids extracted from whole brains and brain EVs from 5XFAD and *fro;*5XFAD mice and astrocytes and astrocyte EVs. Ceramide and cholesterol are used as standards. *F*, Quantification of the ceramide:cholesterol ratios from 5XFAD and *fro;*5XFAD brain and brain EVs as shown in *E* (*n* = 3; Student's *t* test). *G*, Quantification of ceramide from thin-layer chromatographs of 5XFAD and *fro;*5XFAD brain EVs normalized to protein (*n* = 2; Student's *t* test). *H*, Western blot of exosome marker Alix from 5XFAD and *fro;*5XFAD sera after ExoQuick isolation (left) or ultracentrifugation (right). *I*, Quantification of Alix band intensity in H (*n* = 3; Student's *t* test). All quantitative data shown are means ± SEM.

gomyelin (Fig. 4*I*). However, 5XFAD mice showed 2.0- to 2.5-fold more serum anti-C18:0, C24:1, and C16:0 IgG activity than WT and *fro* mice. The *fro;*5XFAD mice also had significantly lower anti-C18:0 and C24:1 (but not C16:0) ceramide IgG than 5XFAD mice (Fig. 4*J*–*L*).
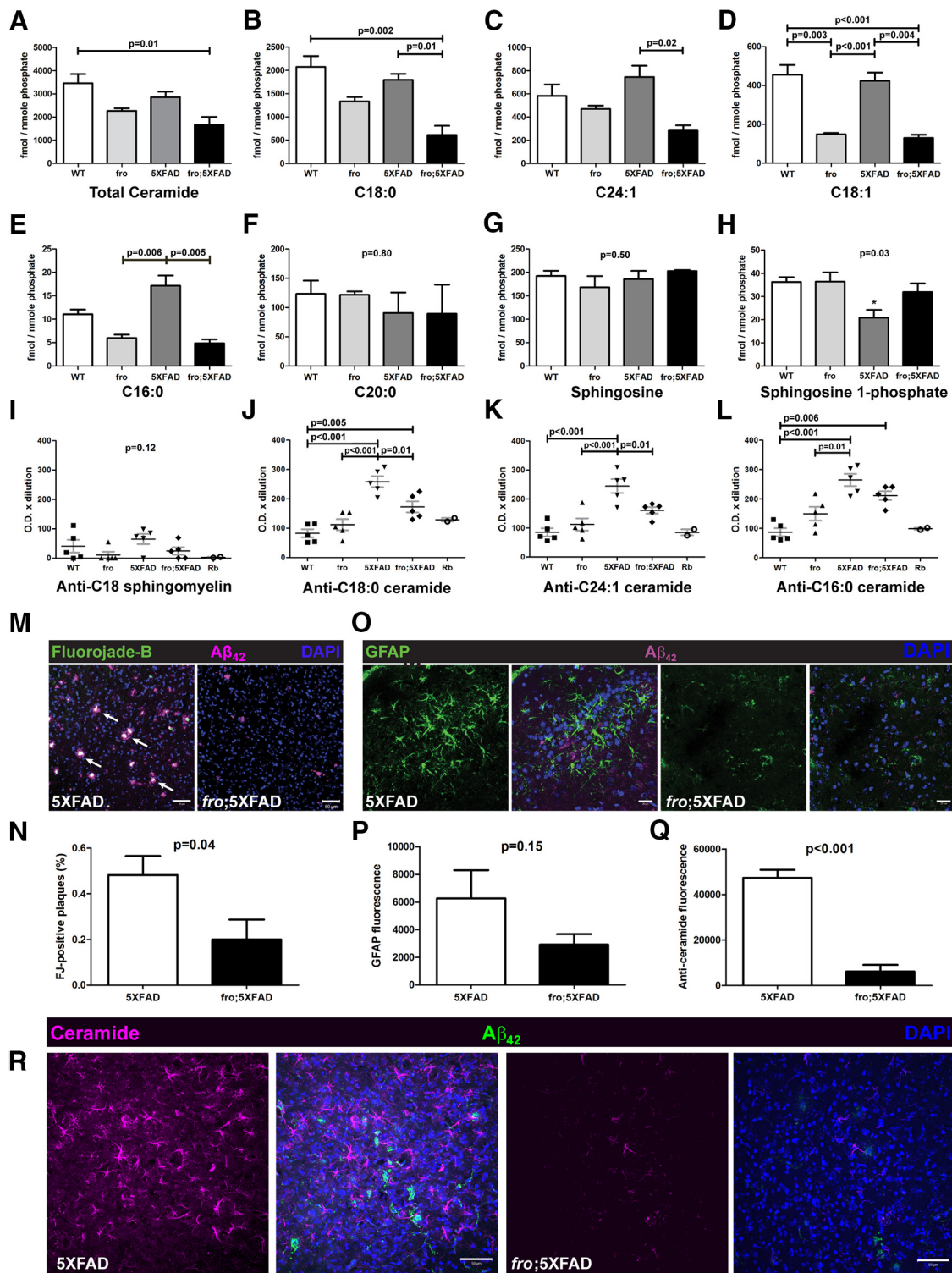
Neuronal degeneration and astrocyte activation is reduced in *fro;*5XFAD mice
Neuronal degeneration and astrocyte activation are both hallmarks of AD. We used the FluoroJade B (FJB) to label degenerating neurons (Schmued and Hopkins, 2000) and anti-GFAP to label astrocytes in the retrosplenial and entorhinal cortex and hippocampus of 10-month-old 5XFAD and *fro;*5XFAD brains in conjuction with anti-Aβ₄₂ to visualize plaques. FJB labeling was present in plaques of 5XFAD (>50% association) mice and in *fro;*5XFAD mice to a lesser extent (<20%; Fig. 4*M,N*). We confirmed that FJB was indeed labeling degenerating neurons rather than activated astrocytes (Damjanac et al., 2007), as verified by presence of NeuN and the absence of GFAP colabeling (images not shown). The *fro;* 5XFAD cortex and hippocampus exhibited a 50% reduction in GFAP immunoreactivity compared with the 5XFAD litter-

mates (Fig. 4*O,P*). Because ceramide elevation is associated with neuronal degeneration and astrocyte activation (Toman et al., 2000; Toman et al., 2002; Jana et al., 2009; Wang et al., 2012; Gu et al., 2013), we also examined ceramide in 5XFAD brain sections and found that *fro;*5XFAD had an 85% reduction in ceramide immunoreactivity, as determined using anti-ceramide antibody (Fig. 4*Q,R*).

Soluble and total Aβ₄₂ levels and plaque burden in 5XFAD and *fro;*5XFAD mice
The 5XFAD model generates mostly Aβ₄₂ (Oakley et al., 2006). We tested soluble (includes oligomeric species) and total (includes plaques) Aβ₄₂ levels by ELISA at 3 time points, 3, 5, and 10 months of age, in males and females. Aβ₄₂ levels were relatively lower (<20%) at 3 months and comparable between 5XFAD and *fro;*5XFAD. At 5 months, as noted in our previous studies (Dinkins et al., 2014; Dinkins et al., 2015), female 5XFAD mice had >2-fold higher levels of total and soluble Aβ₄₂ compared with males regardless of genotype (data not shown). Compared with 5XFAD, soluble Aβ₄₂ was comparable in male and female *fro;*5XFAD, but total Aβ₄₂ in brain was reduced by 50% in male, but not female, *fro;*5XFAD (*p* = 0.05,

Figure 4. Reduced total brain ceramides, serum anticeramide IgG, degenerating neurons, and astrocyte activation in *fro;*5XFAD mice. *A*–*H*, Liquid chromatography and dual-mass spectrometry analysis of indicated ceramides and sphingosines in WT, *fro*, 5XFAD, and *fro;*5XFAD mice brain ($n = 3$ each; one-way ANOVA with Bonferroni *post hoc* test). *I*–*L*, Quantification of lipid ELISAs to determine relative serum titers of indicated anticeramide IgG in WT, *fro*, 5XFAD, and *fro;*5XFAD mice ($n = 5$ each; one-way ANOVA with Bonferroni's *post hoc* test). *M*, Confocal micrographs of brain tissue from 10-month-old 5XFAD and *fro;*5XFAD mice labeled with FJB to label degenerating neurons and anti-Aβ_{42}. *N*, Quantification of FJB from *M* ($n = 8$; Student's *t* test). *O*, Confocal micrographs of brain tissue from 10-month-old 5XFAD and *fro;*5XFAD mice immunolabeled with anti-GFAP and anti-Aβ_{42}. *P*, Quantification of GFAP immunolabeling from *O* ($n = 6$; Student's *t* test). *Q*, Quantification of anticeramide immunolabeling from *R* ($n = 3$; Student's *t* test). *R*, Confocal micrographs of brain tissue from 10-month-old 5XFAD and *fro;*5XFAD mice immunolabeled with anticeramide and anti-Aβ_{42}. Scale bars: *M*, *R*, 50 μm; *O*, 20 μm. All quantitative data shown indicate means $\pm$ SEM.
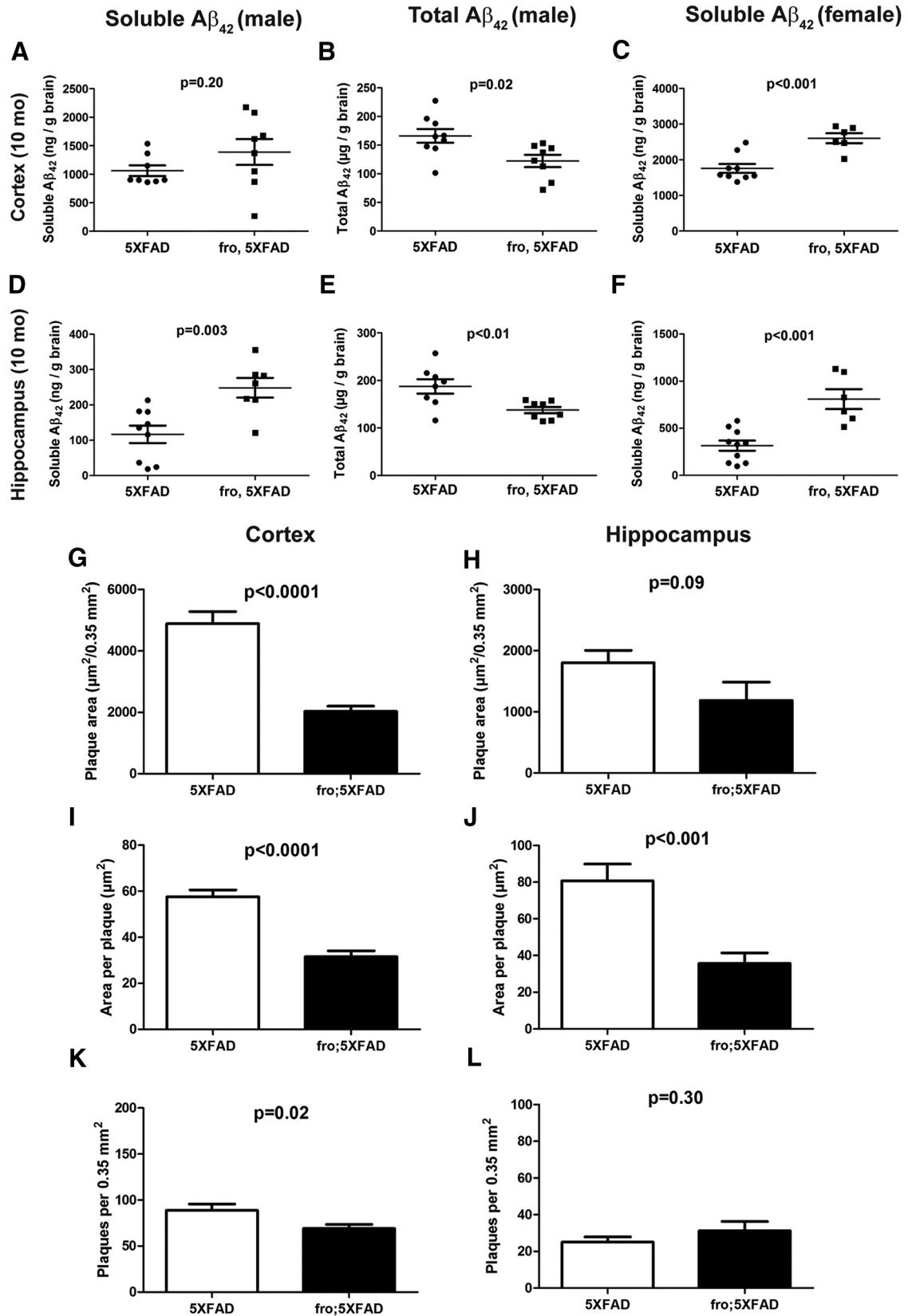
Figure 5. Total $A\beta_{42}$ and plaque loads are reduced in *fro;*5XFAD males, whereas soluble $A\beta_{42}$ is increased. ***A–F***, Dot plots of $A\beta_{42}$ ELISA data from brains of 5XFAD and *fro;*5XFAD mice at 10 months (sex and soluble vs total $A\beta$ indicated in figure). The number (*n*) of mice in each group is indicated by the number of dots in each group (e.g., *n* = 8 for 5XFAD in ***A***). ***G–L***, Graphs showing total plaque area (***G, H***), average plaque size (***I, J***), and plaque counts (***K, L***) per 0.35 mm² (*n* = 5 male mice for each group; 4 images from each region: retrosplenial, somatosensory, motor, and auditory; 5 mice × 4 regions × 4 images = 80 images). All data shown are presented means ± SEM and were analyzed by Student's *t* test.
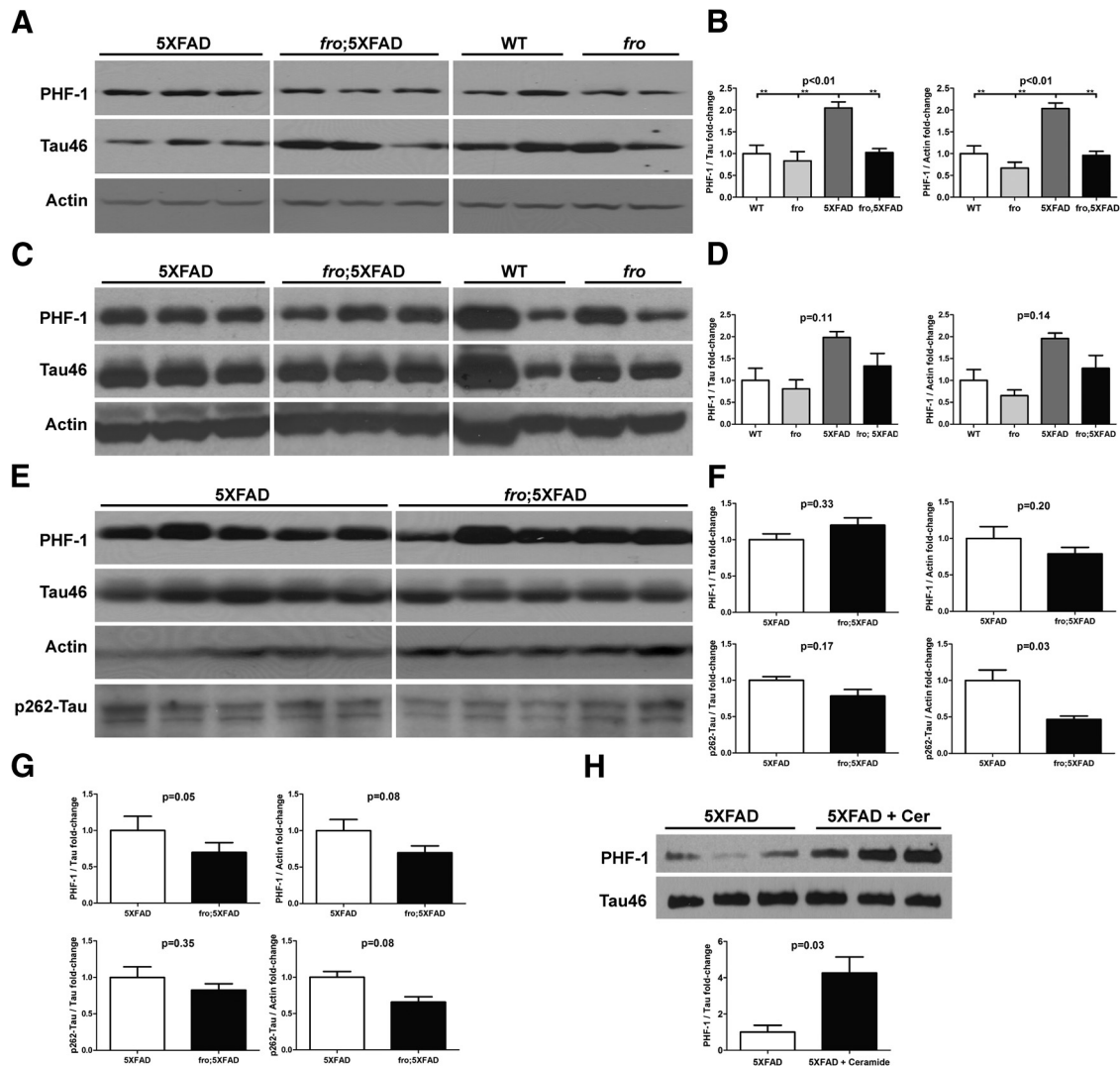
Figure 6. p-tau ratios are reduced in *fro;*5XFAD and increased in 5XFAD mice treated with ceramide. ***A***, ***C***, ***E***, Western analyses of 5XFAD and *fro;*5XFAD brain at 3 (***A***), 5 (***C***), and 10 (***E***) months of age. Homogenates were probed with antibodies against pS396/404-tau (PHF-1), p262-tau, tau (Tau46), and actin. ***B***, ***D***, ***F***, Quantification of p-tau to tau or p-tau to actin ratios from blots in ***A*** (*n* = 3; one-way ANOVA with Bonferroni *post hoc* test), ***C*** (*n* = 3; one-way ANOVA with Bonferroni *post hoc* test), and ***E*** (*n* = 5; Student's *t* test), respectively. In ***G***, the data for hippocampi are presented, but blots are not shown (*n* = 5; Student's *t* test). ***H***, Western blot analysis of p-tau (PHF-1) and tau in cortices of 5XFAD mice injected with Freund's adjuvant with and without C18:0 ceramide and quantification of band intensity in ***H*** (bottom; *n* = 3; Student's *t* test). Quantitative data are presented as means ± SEM. All samples within a comparison group were run on the same gel and cropped for the figure.

n = 9 5XFAD, *n* = 7 *fro;*5XFAD; data not shown). Consistent with Aβ ELISA measurements, all mice expressing the 5XFAD transgenes (with or without the *fro* allele) exhibited plaque pathology by 5 months, whereas total cortical plaque areas were reduced in association with *fro* by 30% in males (but not females, data not shown).

Differences between 5XFAD and *fro;*5XFAD were more pronounced at 10 months of age. In *fro;*5XFAD mice, soluble Aβ$_{42}$ was elevated in cortex (males 25%, females 50%; Fig. 5*A*,*C*) and hippocampus (males 110%, females 250%; Fig. 5*D*,*F*), assayed independently, over 5XFAD mice. Consistent with 5-month-old mice, however, total Aβ$_{42}$ levels were reduced in male *fro;*5XFAD mice only (~30% in cortex and hippocampus; Fig. 5*B*,*E*), and females showed no differences between genotypes (data not shown). With the exception of plaque number in the hippocampus (Fig. 5*L*) in 10-month-old mice, male *fro;*5XFAD showed marked reduction in plaque burden in total plaque area and average plaque size in cortex

and hippocampus (Fig. 5*G*–*J*) and total plaque number in cortex (Fig. 5*K*). Consistently, females showed no differences between 5XFAD and *fro;*5XFAD genotypes in any parameter (data not shown). Mean cortical plaque area values were measured separately in multiple cortical subregions: retrosplenial, somatosensory, motor, and auditory. When analyzed separately according to region, the data follow the same trend: *fro;*5XFAD males, but not females, show significant reductions ($p < 0.01$ in all cases) in plaque area and size (individual data not shown).

*fro;*5XFAD mice have reduced p-tau levels

We also assessed tau phosphorylation (p-tau) in male 5XFAD and *fro;*5XFAD mice at 3, 5, and 10 months of age. At 3 months of age, 5XFAD showed a 2-fold increase in p-tau (pS396/404; PHF-1) relative to phosphorylation-independent tau and actin over WT, *fro*, and *fro;*5XFAD mice, the latter of which was not different from WT or *fro* mice (Fig. 6*A*,*B*). Similar results

were obtained with mice at 5 months of age, although somewhat more variable (Fig. 6C,D). At 10 months of age, we assayed cortex and hippocampus to evaluate PHF-1 and pS262-tau. No statistically significant changes were noted in cortex when normalized to total tau although when normalized to actin, there were reductions in *fro;*5XFAD mice (Fig. 6E,F) at both phosphorylation sites. The reduction in *fro;*5XFAD mice compared with 5XFAD was more pronounced; however, in the hippocampus (Fig. 6G, blots not shown). In a previous study, we treated 3-month-old 5XFAD mice with C18:0 ceramide to stimulate an anticeramide immune response (Dinkins et al., 2015). Ceramide treatment increased the ceramide concentration in whole-brain tissue by 1.5-fold from 3 to 4.5 ng/μg protein ($p < 0.01$, $n = 3$, Student's t test), although the mechanism for this increase is unclear. Consistent with elevated ceramide levels, we found that whole brains from ceramide-treated 5XFAD mice had a 4-fold increase in pS396/404-tau over vehicle-treated mice (PHF-1; Fig. 6H). These mice also had increased serum exosomes and increased plaque burden in the cortex (Dinkins et al., 2015), but we were unable to harvest brain EVs.

Loss of nSMase2 restores cognitive behavior in a fear-conditioning assessment

To assess memory-related behaviors in the mice, we performed context and cue-dependent fear-conditioning experiments in 8-month-old male mice (Dineley et al., 2002). Freezing behavior was defined as the absence of all movement except respiration and facial muscle movement (e.g., whisker twitching). In this test, mice were trained to associate a context (the environment) with a conditioned acoustic stimulus (or cue) and unconditioned electric foot-shock stimulus. 5XFAD males showed reduced freezing behavior (50% reduction) during training compared with WT and *fro* and, to a lesser extent, *fro;*5XFAD mice (Fig. 7A). For contextual fear memory, 5XFAD mice showed a learning deficit (3-fold reduction in freezing behavior) compared with WT and *fro* mice. *fro;*5XFAD mice performed similarly to the WT mice (Fig. 7B). To evaluate cued fear memory, mice were placed in a novel environment and presented with an acoustic stimulus. Compared with WT, 5XFAD demonstrated a 35% reduction in freezing behavior, whereas *fro;*5XFAD were similar (Fig. 7C). These data suggest that reduction of ceramide due to nSMase2 deficiency alleviates the behavioral phenotype in 5xFAD mice. To verify that the expression of 5XFAD transgenes and/or the *fro* genotype was not associated with altered sensory perception, shock sensitivity testing was assessed in all mice for validation. There were no significant differences among WT, 5XFAD, and *fro;*5XFAD mice in their threshold to vocalize, flinch, or move in response to shock intensity. Only discrete differences in the threshold to ambulate in response to shock intensity as associated with *fro* mice directly compared with 5XFAD mice (Fig. 7D). Freezing behavior values, averaged into 1 min bins, are also shown (Fig. 7E,G, respectively, for training, contextual, and cued tests) to confirm that mice exhibited normal exploratory behavior in the absence of stimuli, conditioned or unconditioned, especially during training and cued testing.

Discussion

In this study, we greatly expand on previous work to determine the role of exosomes in Aβ42 aggregation and AD progression. Although Aβ has been challenged as the causative agent of AD and other complexities have been uncovered (Herrup, 2015), the amyloid cascade hypothesis (Hardy and Higgins, 1992) domi-nates as the mechanism underlying the etiology of AD (Musiek and Holtzman, 2015). In addition to genetic evidence from deterministic genes, Aβ aggregation appears to be a triggering mechanism for developing AD (Manelli et al., 2004; Castellano et al., 2011; Garai et al., 2014). Cognitively normal and AD patients produce Aβ at similar rates, but AD patients have reduced clearance (Mawuenyega et al., 2010). We propose that reduced Aβ clearance allows for exosomes/EVs in the brain to interact with Aβ and promote its aggregation by acting as a seed (Meyer-Luehmann et al., 2006; Yuyama et al., 2008; Vingtdeux et al., 2012).

Although this study does not address the molecular component(s) of exosomes that enhances Aβ aggregation, we do note key differences in our data from previous reports. N2a-derived exosomes were shown previously to drive Aβ aggregation, a process that is blocked by endoglycoceramidase digestion, which removes oligosaccharides conjugated to ceramide (Ito and Yamagata, 1986; Yuyama et al., 2012). We show that an anticeramide antibody was able to block Aβ aggregation using ZetaView NTA, in agreement with a previous result (Dinkins et al., 2014). We also show that astrocyte-derived exosomes promote oligomerization at various molecular weights, as well as larger species, whereas another report showed N2a exosomes blocking oligomerization of Aβ (Yuyama et al., 2012). Also, in contrast to our data, published work shows that astrocyte exosomes do not bind Aβ, presumably due to a lower amount of GM1 relative to neuronal exosomes (Yuyama et al., 2015). Our data show GM1 enrichment in astroglial exosomes compared with parent cells. However, even if GM1 is not involved in exosomal Aβ aggregation, cellular prion protein is another candidate involved in Aβ sequestration (An et al., 2013) and aggregation by exosomes (Falker et al., 2016). With respect to *in vitro* glial amyloid clearance assays, our results with astroglial exosomes differ from the study by Yuyama et al. (2012) using neuronal exosomes that promoted Aβ clearance by microglia. Our data showing decreased internalized Aβ are consistent with a role for EVs in promoting extracellular aggregation. Our data using pacFA-ceramide-loaded EVs indicate that the majority of exosome-associated Aβ remains attached at the cell surface, which was eliminated by trypsin before harvesting cells. Indeed, earlier reports define a number of potential interacting molecules for Aβ with the glial cell surface (Verdier et al., 2004).

Published data largely indicate increases in ceramides in human AD and in AD models (Alessenko et al., 2004; Satoi et al., 2005; Marks et al., 2008; Wang et al., 2008; Filippov et al., 2012), with serum ceramide levels being predictive of AD and memory impairment (Mielke et al., 2010; Mielke et al., 2012; Xing et al., 2016). Ceramide has been shown to play roles in promotion of BACE-1 stability (Puglielli et al., 2003), Aβ generation (Geekiyanage and Chan, 2011), and apoptosis in oligodendrocytes (Lee et al., 2004), neurons (Malaplate-Armand et al., 2006; Jana and Pahan, 2010), and astrocytes (Wang et al., 2012). We found that the 5XFAD mice do not exhibit elevated ceramides over nontransgenic controls, suggesting that Aβ alone is not sufficient to elevate ceramide levels. Although it is known that nSMase2 is activated by Aβ to generate ceramide on demand (Malaplate-Armand et al., 2006; Jana and Pahan, 2010; Wang et al., 2012), loss of nSMase2 function in an AD model has not been reported. To address this gap, we generated the *fro;*5XFAD mouse, which lacks nSMase2 activity (Aubin et al., 2005). Because nSMase2 is reported to drive
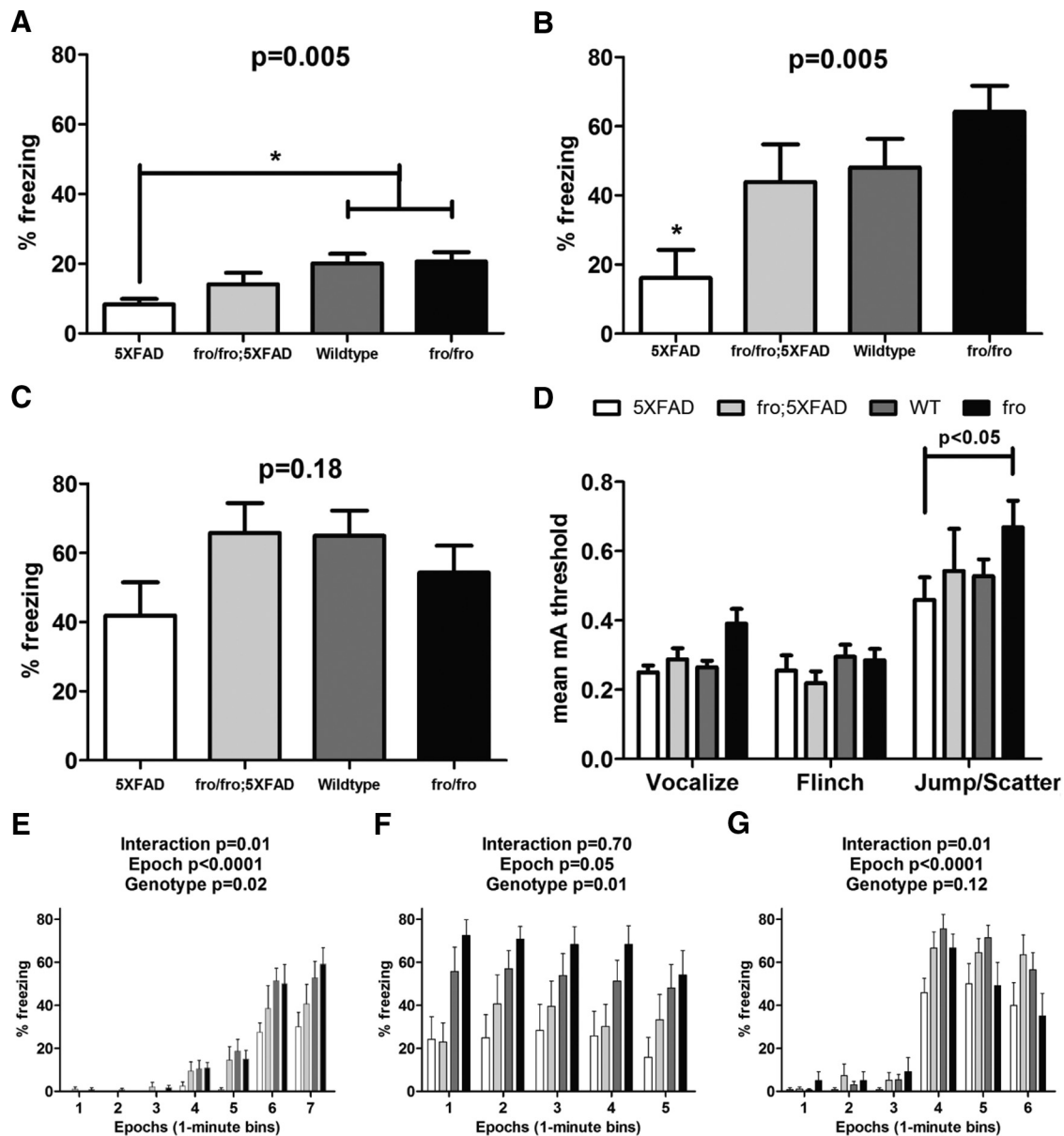
Figure 7. Male *fro;*5XFAD mice show improved fear-conditioned memory at 8 months. *A–C*, Graphs showing means ± SEM of freezing behavior associated with training (*A*) and both contextual (*B*) and cued (*C*) fear-conditioned learning in WT (*n* = 13), *fro* (*n* = 9), 5XFAD (*n* = 9), and *fro;*5XFAD (*n* = 7) mice analyzed by one-way ANOVA with Bonferroni's *post hoc* test. *D*, Graph showing the mean (±SEM) threshold (reported in milliamp units) required to elicit vocalization, flinching, and jumping in response to the presentation electric stock stimuli (range = 0.1–1.0 mA). *E–G*, Graphs showing means ± SEM of freezing behavior presented as the percentage of time mice were frozen in epochs of 1 min bins during training (*A*), contextual testing (*B*), and cued testing (*C*). Data were analyzed by two-way ANOVA with Bonferroni *post hoc* test.

exosome formation in neural cells (Trajkovic et al., 2008; Yuyama et al., 2012; Dinkins et al., 2014; Asai et al., 2015), *fro* mice were expected to have reduced exosome levels in the brain parenchyma. Indeed, we report that *fro* astrocytes do not secrete exosomes in response to Aβ and also show that total brain EVs were reduced by at least 50%, as well as Alix-positive EVs in the serum. We focused our *in vitro* experiments on astrocyte exosomes after finding that astrocytes from the PS1 mouse brain have highly elevated ceramide levels (Wang et al., 2008). Although we found that astrocyte exosomes promote aggregation and block glial clearance of Aβ, we cannot exclude the contribution of exosomes from other neural cell types in classical AD pathology. Indeed, Yuyama et al. (2012) have shown exosomes from primary neurons also promoted Aβ aggregation. We reported previously that cultured primary

neurons secrete exosomes constitutively without stimulation from Aβ, but that exosome secretion could be blocked with the nSMase2 inhibitor GW4869 (Dinkins et al., 2014). These results were in agreement with other published work with neurons (Fauré et al., 2006) suggesting that neuronal and microglial exosomes (Asai et al., 2015) are all reduced in the *fro;*5XFAD model and that all exosomes may contribute to AD pathology in a similar manner. Mice homozygous for the *fro* mutation also exhibited reduced levels of total brain ceramides, in particular the most abundant species found in astrocyte exosomes, C18:0 and C24:1 (Wang et al., 2012). In contrast to ceramides, the reverse occurs with the neuroprotective lipid S1P because 5XFAD mice had an ~40% reduction in brain S1P levels, whereas *fro;*5XFAD mice were similar to WT and *fro* mice. It has been shown that S1P levels are reduced

in AD patients (He et al., 2010; Couttas et al., 2014), which may contribute to increased neuronal degeneration.

We reported previously that 5XFAD mice exhibit an age-dependent increase in anticeramide IgG that occurs to a lesser extent in aging nontransgenic mice (Dinkins et al., 2015). Here, 5XFAD mice showed considerable increases in IgG recognizing C18:0, C24:1, and C16:0, which was reduced in the *fro*;5XFAD mice. Exosomes can modulate the immune system in various contexts (Prado et al., 2008; Okoye et al., 2014; Bretz et al., 2013), including the induction of IgG2b production by EVs loaded with α-galactosylceramide (Gehrmann et al., 2013). Because *fro*;5XFAD mice showed reduced Alix levels in serum exosomes, these mice may have decreased anticeramide IgG titers as a result of fewer circulating exosomes, as postulated in our previous work (Dinkins et al., 2015).

The *fro*;5XFAD mice showed improvements with respect to total $A\beta_{42}$. Male *fro*;5XFAD mice had lower total $A\beta_{42}$ levels than 5XFAD controls at 5 and 10 months in the cortex and hippocampus, consistent with our short-term study using the nSMase2 inhibitor GW4869 on 3-month-old mice (Dinkins et al., 2014). Female 5XFAD mice had $A\beta_{42}$ levels that were approximately double that of males and *fro*;5XFAD females had no significant reduction in their total $A\beta_{42}$ (Dinkins et al., 2014; Dinkins et al., 2015). In contrast, the amount of soluble $A\beta_{42}$ in both sexes was higher in *fro*;5XFAD mice compared with 5XFAD. We interpret this finding to be consistent with our hypothesis that EVs promote $A\beta$ aggregation by binding low-molecular-weight $A\beta$ species. If the total EV levels are reduced, a larger proportion of $A\beta$ remains soluble and easier to clear by either glia or LRP1-mediated transport across the BBB (Shibata et al., 2000; Deane et al., 2008; Storck et al., 2016). Increased soluble $A\beta$ concentration, most likely oligomers, seems contradictory to the notion that $A\beta$ oligomers are the most neurotoxic $A\beta$ conformation (Lambert et al., 1998; Baleriola et al., 2014). If exosomes act to sequester $A\beta$ oligomers (An et al., 2013; Hong et al., 2014; Falker et al., 2016), then a reduction in total exosome levels would be expected to increase the amount of soluble $A\beta$ proportionally. Histochemical analysis of plaques is also a useful metric as a measure of brain $A\beta$ content. Overall plaque burden (total area and average size) was decreased in male, but not female, *fro*;5XFAD mice compared with 5XFAD mice in the cortex and hippocampus. It is thought that tau-related pathology occurs downstream of $A\beta$ aggregation (Musiek and Holtzman, 2015). We found 5XFAD mice to have a higher proportion of pS396/404-tau to total tau and actin in 3- to 5-month old mice compared with WT and *fro*;5XFAD mice. In 10-month-old *fro*;5XFAD mice, there were consistently lower hippocampal p-tau ratios, although older *fro*;5XFAD mice had reduced cortical p-tau to actin ratio. Consistent with the proposed role of ceramide-enriched exosomes in increasing tau phosphorylation, elevation of ceramide concentration in brain tissue by ceramide treatment of 5XFAD mice led to increased p-tau ratios. In agreement with our findings, blocking exosome secretion with GW4869 to inhibit nSMase prevented the spread of pathological tau in a mouse model, indicating a role for EVs in AD progression (Asai et al., 2015).

Our contextual fear-conditioning data are consistent with other published reports showing deficits in 5XFAD males (Kimura and Ohno, 2009; Kaczorowski et al., 2011). Our shock sensitivity and epoch-aggregated data indicate that *fro* mice do not have increased sensitivity to the test conditions. To our knowledge, the only report assessing the role of

nSMases, predominantly nSMase2, in brain, behavior, or memory showed that inhibition of nSMase2 with GW4869 impaired spatial navigation maze learning (Tabatadze et al., 2010). Our results not only show that genetic nSMase2 deficiency in an AD mouse model improves memory as it relates to fear conditioning, but also that the *fro* nontransgenics had slightly better performance, suggesting a role for nSMase2 and ceramide in learning and memory function, particularly associative learning. In conclusion, we provide evidence that ceramide-enriched exosomes play a role in the accumulation of $A\beta$ *in vivo* and that reducing exosome secretion by genetic lesion of the *fro* mouse ameliorates AD-associated pathology and improves cognition.

References

Alessenko AV, Bugrova AE, Dudnik LB (2004) Connection of lipid peroxide oxidation with the sphingomyelin pathway in the development of Alzheimer's disease. Biochem Soc Trans 32:144–146. CrossRef Medline

An K, Klyubin I, Kim Y, Jung JH, Mably AJ, O'Dowd ST, Lynch T, Kanmert D, Lemere CA, Finan GM, Park JW, Kim TW, Walsh DM, Rowan MJ, Kim JH (2013) Exosomes neutralize synaptic-plasticity-disrupting activity of Abeta assemblies in vivo. Mol Brain 6:47. CrossRef Medline

Asai H, Ikezu S, Tsunoda S, Medalla M, Luebke J, Haydar T, Wolozin B, Butovsky O, Kügler S, Ikezu T (2015) Depletion of microglia and inhibition of exosome synthesis halt tau propagation. Nat Neurosci 18:1584–1593. CrossRef Medline

Aubin I, Adams CP, Opsahl S, Septier D, Bishop CE, Auge N, Salvayre R, Negre-Salvayre A, Goldberg M, Guénet JL, Poirier C (2005) A deletion in the gene encoding sphingomyelin phosphodiesterase 3 (Smpd3) results in osteogenesis and dentinogenesis imperfecta in the mouse. Nat Genet 37:803–805. CrossRef Medline

Baleriola J, Walker CA, Jean YY, Crary JF, Troy CM, Nagy PL, Hengst U (2014) Axonally synthesized ATF4 transmits a neurodegenerative signal across brain regions. Cell 158:1159–1172. CrossRef Medline

Bertram L, Tanzi RE (2008) Thirty years of Alzheimer's disease genetics: the implications of systematic meta-analyses. Nat Rev Neurosci 9:768–778. CrossRef Medline

Bretz NP, Ridinger J, Rupp AK, Rimbach K, Keller S, Rupp C, Marmé F, Umansky L, Umansky V, Eigenbrod T, Sammar M, Altevogt P (2013) Body fluid exosomes promote secretion of inflammatory cytokines in monocytic cells via Toll-like receptor signaling. J Biol Chem 288:36691–36702. CrossRef Medline

Castellano JM, Kim J, Stewart FR, Jiang H, DeMattos RB, Patterson BW, Fagan AM, Morris JC, Mawuenyega KG, Cruchaga C, Goate AM, Bales KR, Paul SM, Bateman RJ, Holtzman DM (2011) Human apoE isoforms differentially regulate brain amyloid-beta peptide clearance. Sci Transl Med 3:89ra57. CrossRef Medline

Couttas TA, Kain N, Daniels B, Lim XY, Shepherd C, Kril J, Pickford R, Li H, Garner B, Don AS (2014) Loss of the neuroprotective factor Sphingosine 1-phosphate early in Alzheimer's disease pathogenesis. Acta Neuropathol Commun 2:9. CrossRef Medline

Damjanac M, Rioux Bilan A, Barrier L, Pontcharraud R, Anne C, Hugon J, Page G (2007) Fluoro-Jade B staining as useful tool to identify activated microglia and astrocytes in a mouse transgenic model of Alzheimer's disease. Brain Res 1128:40–49. CrossRef Medline

Dbaibo GS, Obeid LM, Hannun YA (1993) Tumor necrosis factor-alpha (TNF-alpha) signal transduction through ceramide. Dissociation of growth inhibitory effects of TNF-alpha from activation of nuclear factor-kappa B. J Biol Chem 268:17762–17766. Medline

Deane R, Sagare A, Hamm K, Parisi M, Lane S, Finn MB, Holtzman DM, Zlokovic BV (2008) apoE isoform-specific disruption of amyloid beta peptide clearance from mouse brain. J Clin Invest 118:4002–4013. CrossRef Medline

Dineley KT, Xia X, Bui D, Sweatt JD, Zheng H (2002) Accelerated plaque accumulation, associative learning deficits, and up-regulation of alpha 7 nicotinic receptor protein in transgenic mice co-expressing mutant human presenilin 1 and amyloid precursor proteins. J Biol Chem 277:22768–22780. CrossRef Medline

Dinkins MB, Dasgupta S, Wang G, Zhu G, Bieberich E (2014) Exosome reduction in vivo is associated with lower amyloid plaque load in the

5XFAD mouse model of Alzheimer's disease. Neurobiol Aging 35: 1792–1800. CrossRef Medline

Dinkins MB, Dasgupta S, Wang G, Zhu G, He Q, Kong JN, Bieberich E (2015) The 5XFAD mouse model of Alzheimer's disease exhibits an age-dependent increase in anticeramide IgG and exogenous administration of ceramide further increases anticeramide titers and amyloid plaque burden. J Alzheimers Dis 46:55–61. CrossRef Medline

Falker C, Hartmann A, Guett I, Dohler F, Altmeppen H, Betzel C, Schubert R, Thurm D, Wegwitz F, Joshi P, Verderio C, Krasemann S, Glatzel M (2016) Exosomal PrP drives fibrillization of amyloid beta and counteracts amyloid beta-mediated neurotoxicity. J Neurochem 137:88–100. CrossRef Medline

Fauré J, Lachenal G, Court M, Hirrlinger J, Chatellard-Causse C, Blot B, Grange J, Schoenn G, Goldberg Y, Boyer V, Kirchhoff F, Raposo G, Garin J, Sadoul R (2006) Exosomes are release by cultured cortical neurons. Mol Cell Neurosci 31:642–648. CrossRef Medline

Fiandaca MS, Kapogiannis D, Mapstone M, Boxer A, Eitan E, Schwartz JB, Abner EL, Petersen RC, Federoff HJ, Miller BL, Goetzl EJ (2015) Identification of preclinical Alzheimer's disease by a profile of pathogenic proteins in neurally derived blood exosomes: a case-control study. Alzheimers Dement 11:600–607.e1. CrossRef Medline

Filippov V, Song MA, Zhang K, Vinters HV, Tung S, Kirsch WM, Yang J, Duerksen-Hughes PJ (2012) Increased ceramide in brains with Alzheimer's and other neurodegenerative diseases. J Alzheimers Dis 29:537–547. CrossRef Medline

Folch J, Lees M, Sloane Stanley GH (1957) A simple method for the isolation and purification of total lipides from animal tissues. J Biol Chem 226: 497–509. Medline

Garai K, Verghese PB, Baban B, Holtzman DM, Frieden C (2014) The binding of apolipoprotein E to oligomers and fibrils of amyloid-beta alters the kinetics of amyloid aggregation. Biochemistry 53:6323–6331. CrossRef Medline

Geekiyanage H, Chan C (2011) MicroRNA-137/181c regulates serine palmitoyltransferase and in turn amyloid beta, novel targets in sporadic Alzheimer's disease. J Neurosci 31:14820–14830. CrossRef Medline

Gehrmann U, Hiltbrunner S, Georgoudaki AM, Karlsson MC, Näslund TI, Gabrielsson S (2013) Synergistic induction of adaptive antitumor immunity by codelivery of antigen with alpha-galactosylceramide on exosomes. Cancer Res 73:3865–3876. Medline

Gomez-Muñoz A, Presa N, Gomez-Larrauri A, Rivera IG, Trueba M, Ordonez M (2015) Control of inflammatory responses by ceramide, sphingosine 1-phosphate and ceramide 1-phosphate. Prog Lipid Res 61: 51–62. CrossRef Medline

Gu L, Huang B, Shen W, Gao L, Ding Z, Wu H, Guo J (2013) Early activation of nSMase2/ceramide pathway in astrocytes is involved in ischemia-associated neuronal damage via inflammation in rat hippocampi. J Neuroinflammation 10:109. CrossRef Medline

Guénet JL, Stanescu R, Maroteaux P, Stanescu V (1981) Fragilitas ossium: a new autosomal recessive mutation in the mouse. J Hered 72:440–441. Medline

Guescini M, Genedani S, Stocchi V, Agnati LF (2010) Astrocytes and Glioblastoma cells release exosomes carrying mtDNA. J Neural Transm 117: 1–4. CrossRef Medline

Hardy JA, Higgins GA (1992) Alzheimer's disease: the amyloid cascade hypothesis. Science 256:184–185. CrossRef Medline

Hayashi H, Kimura N, Yamaguchi H, Hasegawa K, Yokoseki T, Shibata M, Yamamoto N, Michikawa M, Yoshikawa Y, Terao K, Matsuzaki K, Lemere CA, Selkoe DJ, Naiki H, Yanagisawa K (2004) A seed for Alzheimer amyloid in the brain. J Neurosci 24:4894–4902. CrossRef Medline

He Q, Wang G, Dasgupta S, Dinkins M, Zhu G, Bieberich E (2012) Characterization of an apical ceramide-enriched compartment regulating ciliogenesis. Mol Biol Cell 23:3156–3166. CrossRef Medline

He X, Huang Y, Li B, Gong CX, Schuchman EH (2010) Deregulation of sphingolipid metabolism in Alzheimer's disease. Neurobiol Aging 31: 398–408. CrossRef Medline

Herrup K (2015) The case for rejecting the amyloid cascade hypothesis. Nat Neurosci 18:794–799. CrossRef Medline

Hong S, Ostaszewski BL, Yang T, O'Malley TT, Jin M, Yanagisawa K, Li S, Bartels T, Selkoe DJ (2014) Soluble Abeta oligomers are rapidly sequestered from brain ISF in vivo and bind GM1 ganglioside on cellular membranes. Neuron 82:308–319. CrossRef Medline

Ito M, Yamagata T (1986) A novel glycosphingolipid-degrading enzyme cleaves the linkage between the oligosaccharide and ceramide of neutral and acidic glycosphingolipids. J Biol Chem 261:14278–14282. Medline

Jana A, Pahan K (2010) Fibrillar amyloid-beta-activated human astroglia kill primary human neurons via neutral sphingomyelinase: implications for Alzheimer's disease. J Neurosci 30:12676–12689. CrossRef Medline

Jana A, Hogan EL, Pahan K (2009) Ceramide and neurodegeneration: susceptibility of neurons and oligodendrocytes to cell damage and death. J Neurol Sci 278:5–15. CrossRef Medline

Joshi P, Benussi L, Furlan R, Ghidoni R, Verderio C (2015) Extracellular vesicles in Alzheimer's disease: friends or foes? Focus on abeta-vesicle interaction. Int J Mol Sci 16:4800–4813. CrossRef Medline

Kaczorowski CC, Sametsky E, Shah S, Vassar R, Disterhoft JF (2011) Mechanisms underlying basal and learning-related intrinsic excitability in a mouse model of Alzheimer's disease. Neurobiol Aging 32:1452–1465. CrossRef Medline

Kimura R, Ohno M (2009) Impairments in remote memory stabilization precede hippocampal synaptic and cognitive failures in 5XFAD Alzheimer mouse model. Neurobiol Dis 33:229–235. CrossRef Medline

Kobayashi Y, Kiguchi N, Maeda T, Ozaki M, Kishioka S (2012) The critical role of spinal ceramide in the development of partial sciatic nerve ligation-induced neuropathic pain in mice. Biochem Biophys Res Commun 421:318–322. CrossRef Medline

Kong JN, Hardin K, Dinkins M, Wang G, He Q, Mujadzic T, Zhu G, Bielawski J, Spassieva S, Bieberich E (2015) Regulation of Chlamydomonas flagella and ependymal cell motile cilia by ceramide-mediated translocation of GSK3. Mol Biol Cell 26:4451–4465. CrossRef Medline

Kosaka N, Iguchi H, Hagiwara K, Yoshioka Y, Takeshita F, Ochiya T (2013) Neutral sphingomyelinase 2 (nSMase2)-dependent exosomal transfer of angiogenic microRNAs regulate cancer cell metastasis. J Biol Chem 288: 10849–10859. CrossRef Medline

Kowal J, Tkach M, Théry C (2014) Biogenesis and secretion of exosomes. Curr Opin Cell Biol 29:116–125. CrossRef Medline

Kowal J, Arras G, Colombo M, Jouve M, Morath JP, Primdal-Bengtson B, Dingli F, Loew D, Tkach M, Théry C (2016) Proteomic comparison defines novel markers to characterize heterogeneous populations of extracellular vesicle subtypes. Proc Natl Acad Sci U S A 113:E968–E977. CrossRef Medline

Krishnamurthy K, Dasgupta S, Bieberich E (2007) Development and characterization of a novel anticeramide antibody. J Lipid Res 48:968–975. CrossRef Medline

Lambert MP, Barlow AK, Chromy BA, Edwards C, Freed R, Liosatos M, Morgan TE, Rozovsky I, Trommer B, Viola KL, Wals P, Zhang C, Finch CE, Krafft GA, Klein WL (1998) Diffusible, nonfibrillar ligands derived from Abeta1–42 are potent central nervous system neurotoxins. Proc Natl Acad Sci U S A 95:6448–6453. CrossRef Medline

Lee JT, Xu J, Lee JM, Ku G, Han X, Yang DI, Chen S, Hsu CY (2004) Amyloid-beta peptide induces oligodendrocyte death by activating the neutral sphingomyelinase-ceramide pathway. J Cell Biol 164:123–131. CrossRef Medline

Liu B, Hassler DF, Smith GK, Weaver K, Hannun YA (1998) Purification and characterization of a membrane bound neutral pH optimum magnesium-dependent and phosphatidylserine-stimulated sphingomyelinase from rat brain. J Biol Chem 273:34472–34479. CrossRef Medline

Luberto C, Hannun YA (1998) Sphingomyelin synthase, a potential regulator of intracellular levels of ceramide and diacylglycerol during SV40 transformation. Does sphingomyelin synthase account for the putative phosphatidylcholine-specific phospholipase C? J Biol Chem 273:14550–14559. CrossRef Medline

Malaplate-Armand C, Florent-Béchard S, Youssef I, Koziel V, Sponne I, Kriem B, Leininger-Muller B, Olivier JL, Oster T, Pillot T (2006) Soluble oligomers of amyloid-beta peptide induce neuronal apoptosis by activating a cPLA2-dependent sphingomyelinase-ceramide pathway. Neurobiol Dis 23:178–189. CrossRef Medline

Manelli AM, Stine WB, Van Eldik LJ, LaDu MJ (2004) ApoE and Abeta1–42 interactions: effects of isoform and conformation on structure and function. J Mol Neurosci 23:235–246. CrossRef Medline

Marks N, Berg MJ, Saito M, Saito M (2008) Glucosylceramide synthase decrease in frontal cortex of Alzheimer brain correlates with abnormal increase in endogenous ceramides: consequences to morphology and viability on enzyme suppression in cultured primary neurons. Brain Res 1191:136–147. CrossRef Medline

Mathias S, Younes A, Kan CC, Orlow I, Joseph C, Kolesnick RN (1993)

Activation of the sphingomyelin signaling pathway in intact EL4 cells and in a cell-free system by IL-1 beta. Science 259:519–522. CrossRef Medline

Mawuenyega KG, Sigurdson W, Ovod V, Munsell L, Kasten T, Morris JC, Yarasheski KE, Bateman RJ (2010) Decreased clearance of CNS beta-amyloid in Alzheimer's disease. Science 330:1774. CrossRef Medline

Mehdiani A, Maier A, Pinto A, Barth M, Akhyari P, Lichtenberg A (2015) An innovative method for exosome quantification and size measurement. J Vis Exp 95:50974. CrossRef Medline

Meyer-Luehmann M, Coomaraswamy J, Bolmont T, Kaeser S, Schaefer C, Kilger E, Neuenschwander A, Abramowski D, Frey P, Jaton AL, Vigouret JM, Paganetti P, Walsh DM, Mathews PM, Ghiso J, Staufenbiel M, Walker LC, Jucker M (2006) Exogenous induction of cerebral beta-amyloidogenesis is governed by agent and host. Science 313:1781–1784. CrossRef Medline

Mielke MM, Haughey NJ, Bandaru VV, Schech S, Carrick R, Carlson MC, Mori S, Miller MI, Ceritoglu C, Brown T, Albert M, Lyketsos CG (2010) Plasma ceramides are altered in mild cognitive impairment and predict cognitive decline and hippocampal volume loss. Alzheimers Dement 6:378–385. CrossRef Medline

Mielke MM, Bandaru VV, Haughey NJ, Xia J, Fried LP, Yasar S, Albert M, Varma V, Harris G, Schneider EB, Rabins PV, Bandeen-Roche K, Lyketsos CG, Carlson MC (2012) Serum ceramides increase the risk of Alzheimer disease: the Women's Health and Aging Study II. Neurology 79: 633–641. CrossRef Medline

Musiek ES, Holtzman DM (2015) Three dimensions of the amyloid hypothesis: time, space and 'wingmen'. Nat Neurosci 18:800–806. CrossRef Medline

Nikolova-Karakashian MN, Rozenova KA (2010) Ceramide in stress response. Adv Exp Med Biol 688:86–108. CrossRef Medline

Oakley H, Cole SL, Logan S, Maus E, Shao P, Craft J, Guillozet-Bongaarts A, Ohno M, Disterhoft J, Van Eldik L, Berry R, Vassar R (2006) Intraneuronal beta-amyloid aggregates, neurodegeneration, and neuron loss in transgenic mice with five familial Alzheimer's disease mutations: potential factors in amyloid plaque formation. J Neurosci 26:10129–10140. CrossRef Medline

Okoye IS, Coomes SM, Pelly VS, Czieso S, Papayannopoulos V, Tolmachova T, Seabra MC, Wilson MS (2014) MicroRNA-containing T-regulatory-cell-derived exosomes suppress pathogenic T helper 1 cells. Immunity 41:89–103. Medline

Patil S, Melrose J, Chan C (2007) Involvement of astroglial ceramide in palmitic acid-induced Alzheimer-like changes in primary neurons. Eur J Neurosci 26:2131–2141. CrossRef Medline

Perez-Gonzalez R, Gauthier SA, Kumar A, Levy E (2012) The exosome secretory pathway transports amyloid precursor protein carboxyl-terminal fragments from the cell into the brain extracellular space. J Biol Chem 287:43108–43115. CrossRef Medline

Prado N, Marazuela EG, Segura E, Fernández-García H, Villalba M, Théry C, Rodríguez R, Batanero E (2008) Exosomes from bronchoalveolar fluid of tolerized mice prevent allergic reaction. J Immunol 181:1519–1525. CrossRef Medline

Puglielli L, Ellis BC, Saunders AJ, Kovacs DM (2003) Ceramide stabilizes beta-site amyloid precursor protein-cleaving enzyme 1 and promotes amyloid beta-peptide biogenesis. J Biol Chem 278:19777–19783. CrossRef Medline

Qin J, Berdyshev E, Poirer C, Schwartz NB, Dawson G (2012) Neutral sphingomyelinase 2 deficiency increases hyaluronan synthesis by up-regulation of Hyaluronan synthase 2 through decreased ceramide production and activation of Akt. J Biol Chem 287:13620–13632. CrossRef Medline

Rajendran L, Honsho M, Zahn TR, Keller P, Geiger KD, Verkade P, Simons K (2006) Alzheimer's disease beta-amyloid peptides are released in association with exosomes. Proc Natl Acad Sci U S A 103:11172–11177. CrossRef Medline

Record M, Carayon K, Poirot M, Silvente-Poirot S (2014) Exosomes as new vesicular lipid transporters involved in cell-cell communication and various pathophysiologies. Biochim Biophys Acta 1841:108–120. CrossRef Medline

Rubio-Perez JM, Morillas-Ruiz JM (2012) A review: inflammatory process in Alzheimer's disease, role of cytokines. ScientificWorldJournal 2012: 756357. CrossRef Medline

Satoi H, Tomimoto H, Ohtani R, Kitano T, Kondo T, Watanabe M, Oka N, Akiguchi I, Furuya S, Hirabayashi Y, Okazaki T (2005) Astroglial expression of ceramide in Alzheimer's disease brains: a role during neuronal apoptosis. Neuroscience 130:657–666. CrossRef Medline

Schmued LC, Hopkins KJ (2000) Fluoro-Jade B: a high affinity fluorescent marker for the localization of neuronal degeneration. Brain Res 874: 123–130. CrossRef Medline

Shamseddine AA, Airola MV, Hannun YA (2015) Roles and regulation of neutral sphingomyelinase-2 in cellular and pathological processes. Adv Biol Regul 57:24–41. CrossRef Medline

Sharples RA, Vella LJ, Nisbet RM, Naylor R, Perez K, Barnham KJ, Masters CL, Hill AF (2008) Inhibition of gamma-secretase causes increased secretion of amyloid precursor protein C-terminal fragments in association with exosomes. FASEB J 22:1469–1478. CrossRef Medline

Shibata M, Yamada S, Kumar SR, Calero M, Bading J, Frangione B, Holtzman DM, Miller CA, Strickland DK, Ghiso J, Zlokovic BV (2000) Clearance of Alzheimer's amyloid-ss(1–40) peptide from brain by LDL receptor-related protein-1 at the blood-brain barrier. J Clin Invest 106:1489–1499. CrossRef Medline

Storck SE, Meister S, Nahrath J, Meißner JN, Schubert N, Di Spiezio A, Baches S, Vandenbroucke RE, Bouter Y, Prikulis I, Korth C, Weggen S, Heimann A, Schwaninger M, Bayer TA, Pietrzik CU (2016) Endothelial LRP1 transports amyloid-beta1–42 across the blood-brain barrier. J Clin Invest 126:123–136. CrossRef Medline

Tabatadze N, Savonenko A, Song H, Bandaru VV, Chu M, Haughey NJ (2010) Inhibition of neutral sphingomyelinase-2 perturbs brain sphingolipid balance and spatial memory in mice. J Neurosci Res 88:2940–2951. CrossRef Medline

Taylor DD, Zacharias W, Gercel-Taylor C (2011) Exosome isolation for proteomic analyses and RNA profiling. Methods Mol Biol 728:235–246. CrossRef Medline

Toman RE, Spiegel S, Faden AI (2000) Role of ceramide in neuronal cell death and differentiation. J Neurotrauma 17:891–898. CrossRef Medline

Toman RE, Movsesyan V, Murthy SK, Milstien S, Spiegel S, Faden AI (2002) Ceramide-induced cell death in primary neuronal cultures: upregulation of ceramide levels during neuronal apoptosis. J Neurosci Res 68:323–330. CrossRef Medline

Tomiuk S, Zumbansen M, Stoffel W (2000) Characterization and subcellular localization of murine and human magnesium-dependent neutral sphingomyelinase. J Biol Chem 275:5710–5717. CrossRef Medline

Trajkovic K, Hsu C, Chiantia S, Rajendran L, Wenzel D, Wieland F, Schwille P, Brügger B, Simons M (2008) Ceramide triggers budding of exosome vesicles into multivesicular endosomes. Science 319:1244–1247. CrossRef Medline

Verdier Y, Zarándi M, Penke B (2004) Amyloid beta-peptide interactions with neuronal and glial cell plasma membrane: binding sites and implications for Alzheimer's disease. J Pept Sci 10:229–248. CrossRef Medline

Verghese PB, Castellano JM, Garai K, Wang Y, Jiang H, Shah A, Bu G, Frieden C, Holtzman DM (2013) ApoE influences amyloid-beta (Abeta) clearance despite minimal apoE/Abeta association in physiological conditions. Proc Natl Acad Sci U S A 110:E1807–1816. CrossRef Medline

Vingtdeux V, Sergeant N, Buée L (2012) Potential contribution of exosomes to the prion-like propagation of lesions in Alzheimer's disease. Front Physiol 3:229. CrossRef Medline

Wang G, Silva J, Dasgupta S, Bieberich E (2008) Long-chain ceramide is elevated in presenilin 1 (PS1M146V) mouse brain and induces apoptosis in PS1 astrocytes. Glia 56:449–456. CrossRef Medline

Wang G, Dinkins M, He Q, Zhu G, Poirier C, Campbell A, Mayer-Proschel M, Bieberich E (2012) Astrocytes secrete exosomes enriched with proapoptotic ceramide and prostate apoptosis response 4 (PAR-4): potential mechanism of apoptosis induction in Alzheimer disease (AD). J Biol Chem 287:21384–21395. CrossRef Medline

Xing Y, Tang Y, Zhao L, Wang Q, Qin W, Zhang JL, Jia J (2016) Plasma ceramides and neuropsychiatric symptoms of Alzheimer's disease. J Alzheimers Dis 52:1029–1035. CrossRef Medline

Yuyama K, Yamamoto N, Yanagisawa K (2008) Accelerated release of exosome-associated GM1 ganglioside (GM1) by endocytic pathway abnormality: another putative pathway for GM1-induced amyloid fibril formation. J Neurochem 105:217–224. CrossRef Medline

Yuyama K, Sun H, Mitsutake S, Igarashi Y (2012) Sphingolipid-modulated exosome secretion promotes clearance of amyloid-beta by microglia. J Biol Chem 287:10977–10989. CrossRef Medline

Yuyama K, Sun H, Usuki S, Sakai S, Hanamatsu H, Mioka T, Kimura N, Okada M, Tahara H, Furukawa J, Fujitani N, Shinohara Y, Igarashi Y (2015) A potential function for neuronal exosomes: sequestering intracerebral amyloid-beta peptide. FEBS Lett 589:84–88. CrossRef Medline